Max-Planck-Institut
für Mathematik
in den Naturwissenschaften
Leipzig

Wavelet Approach to Quasi Two-Dimensional Extended Many-Particle Systems. I. Supercell Hartree-Fock Method

by

Heinz-Jürgen Flad, Wolfgang Hackbusch, Hongjun Luo, and Dietmar Kolb

Preprint no.: 66 2004

Wavelet Approach to Quasi Two-Dimensional Extended Many-Particle Systems. I. Supercell Hartree-Fock Method

Heinz-Jürgen Flad and Wolfgang Hackbusch
Max-Planck-Institut für Mathematik in den Naturwissenschaften, Inselstr. 22-26, D-04103 Leipzig

Hongjun Luo and Dietmar Kolb
Institut für Physik, Universität Kassel, Heinrich-Plett-Str. 40, D-34132 Kassel

September 29, 2004

Abstract

We propose a wavelet based multiresolution Hartree-Fock method suitable for quasi two-dimensional extended systems. Intended applications are metallic slabs and excitons confined in quantum wells of semiconductor heterostructures. The method uses a periodic supercell approach, which allows for an incorporation of single impurities. Special emphasis has been laid on low rank tensor product decompositions of orbitals, which take into account the strongly anisotropic character of these systems in one direction. Wavelets provide hierarchical bases that can be adapted to the anisotropic behaviour of the orbitals. We discuss some technical features related to the wavelet expansion of Ewald potentials, which are used to describe the interaction between particles. Due to the vanishing moment property of wavelets, we can achieve sparse representations for the quantities involved. An illustrative example for this are jellium slabs, where we discuss various sparsity features of matrices related to Coulomb and exchange potentials. Benchmark calculations for a homogeneous electron gas finally demonstrate the computational feasibility and numerical accuracy of our approach.

1 Introduction

A challenging problem for computational physics and chemistry are strongly anisotropic systems like surfaces of solids or thin layers of various types of materials. Such kind of systems became of considerable technological interest, we just want to mention semiconductor heterostructures, carbon nanotubes or Langmuir-Blodgett films of organic molecules. Many interesting applications in quantum many-particle theory arise from the physics of surfaces and layers. An intrisic feature of these systems is that they extend fairly homogeneously into the directions parallel to the boundary and show a strongly anisotropic behaviour in the direction perpendicular to it. It is this quasi two-dimensional character which makes them diffult to handle in computations. Wavelet based multiresolution analysis provides numerical tools [7, 8, 10], which might help to improve the efficiency of computational many-particle methods for these systems. In solid state physics, wavelets have been intensively studied in the context of *density functional theory* (DFT) [3, 22], see e.g. Refs. [14, 25, 42, 60] for some recent developments. Within the present work, we discuss a multiresolution *Hartree-Fock* (HF) approach to quasi two-dimensional extended systems. Special emphasis has been laid on low rank tensor product approximations of HF orbitals. This has been accomplished by contracting the wavelet basis in the homogeneous directions according to some systematic contraction scheme, which incorporates basic physical insights. Such kind of construction allows us to combine the advantages of systematic basis sets like wavelets with basis sets highly adapted to the properties of the system under consideration. The latter approach has been proven to be extremely successful in quantum chemistry, where Gaussian-type basis functions enable accurate HF calculations with comparatively small basis sets [26]. Although we limit ourselves in the present work to the HF method, it should be mentioned

that from a computational point of view this method has much in common with more sophisticated many-particle theories, which enable a treatment of electron correlations. It is due to the exchange operator that HF requires the computation of two-electron integrals with respect to the Coulomb interaction. These integrals serve as a starting point for post HF calculations. The standard post HF methods in quantum chemistry, like many-body perturbation theory or the coupled cluster method, require no additional two-electron integrals beyond those already present from a HF calculation. This is not the case for our envisaged treatment of electron correlations within multiresolution analysis [18, 19, 36]. However, we can make use of the algorithms, already implemented for the HF method, to calculate the additional two-electron integrals. In this sense HF serves as a benchmark problem for the development of more sophisticated many-particle methods using wavelet bases.

Conventional metallic surfaces attracted considerable interest in computational physics and have been considered as an important benchmark problem for DFT. A simplified approach to metallic surfaces and slabs is the jellium model where nuclear charges are smeared out into a uniform positive background charge-density, which abruptly discontinues at the surface. Starting with Lang and Kohn's seminal paper [32], jellium surfaces have been extensively studied for various kinds of density functionals [13, 24, 33, 45, 46, 63]. They proved to be of considerable significance for the development of new density functionals. Therefore a strong need for accurate many-body benchmark calculations exists. Remarkably, there are essentially only two many-particle methods that can deal with jellium surfaces, namely *quantum Monte Carlo* (QMC) [1, 34] and the *Fermi hypernetted-chain* (FHNC) method [30, 31]. It exists an ongoing controversy concerning the accuracy of these calculations [41]. Significant deviations with respect to results obtained from DFT calculations [2, 62] exist and presently the reasons for these discrepancies have not been completely settled.

Conduction electrons in semiconductor heterostructures provide an analogous problem on a different energy- and length-scale. The characteristic length-scales of semiconductor layers are between one to two orders of magnitude larger than the typical atomic length-scale. Presently, this makes atomistic many-particle calculations almost impracticable. Nevertheless quantum effects play a prominant role for example in the design of optoelectronic devices [9]. Using the concept of quasi-particles with effective masses, interesting optical properties of semiconductors can be described by effective model Hamiltonians rather similar to those encountered for metallic systems. A new feature arises from the presence of a second species of quasi-particles, these are the holes associated to conduction electrons. Due to comparable effective masses of both species, the Born-Oppenheimer approximation is not applicable and a simultaneous treatment of electrons and holes in many-particle calculations becomes necessary. These excitonic systems share several common features with ordinary atoms and molecules. In excitonic systems, electrons and holes interact via modified Coulomb interactions. The corresponding Schrödinger equation in SI units

$$\left[H_e + H_h + E_g - \sum_{i=1}^{N_e} \sum_{j=1}^{N_h} \frac{e^2}{4\pi\epsilon |\mathbf{r}_{e,i} - \mathbf{r}_{h,j}|} \right] \Psi\left(\mathbf{r}_{e,1} \ldots, \mathbf{r}_{h,1} \ldots\right) = E\, \Psi\left(\mathbf{r}_{e,1} \ldots, \mathbf{r}_{h,1} \ldots\right), \tag{1}$$

$$H_e = \sum_{i=1}^{N_e} \left(-\frac{\hbar^2}{2m_e} \Delta_i + V_e(\mathbf{r}_{e,i}) \right) + \sum_{i<j} \frac{e^2}{4\pi\epsilon |\mathbf{r}_{e,i} - \mathbf{r}_{e,j}|}, \tag{2}$$

$$H_h = \sum_{i=1}^{N_h} \left(-\frac{\hbar^2}{2m_h} \Delta_i + V_h(\mathbf{r}_{h,i}) \right) + \sum_{i<j} \frac{e^2}{4\pi\epsilon |\mathbf{r}_{h,i} - \mathbf{r}_{h,j}|}, \tag{3}$$

where $\mathbf{r}_{e,i}$, $\mathbf{r}_{h,i}$ denote electron and hole coordinates, respectively, looks very much like for a pure many-electron system except that electrons and holes attract each other. The simplest excitons consist of a single electron-hole pair. Under certain circumstances, these excitons combine with each other to form biexcitons or even exciton molecules [50]. Of special interest are biexcitons confined in quantum wells formed by semiconductor heterostructures or quantum dots. For nanostructured materials, the diameter of excitons becomes comparable to the thickness of a layer, which means that the properties of these systems lie

somewhere in between that of free 2d- and 3d-excitons [9]. Therefore these excitons provide interesting two-scale problems, that can be handled similar to jellium slabs. Various types of computational methods have been already applied to excitonic systems. Many-particle effects were treated by DFT [43, 47, 61] or by variational methods [6, 28, 29]. A straightforward application of DFT methods, however, is hampered by a lack of knowledge concerning the detailed form of the exchange-correlation potential for excitons. The construction of such a potential requires some input from many-body calculations for a convenient reference system, as it is the case with the homogeneous electron gas in quantum chemistry. Variational methods are either based on an ad hoc ansatz for the wavefunction [29] with only a small number of variational parameters or used linear expansions in one-particle basis sets similar to standard methods in quantum chemistry [6, 28].

2 Supercell approach to electronic structure calculations

The standard approach to HF electronic structure calculations for infinite periodic systems is based on Bloch orbitals [44]. These orbitals are defined according to Bloch's theorem by their translational symmetry. Furthermore, Bloch orbitals can be used within many-body perturbation theory [4, 57, 58] and coupled cluster theory [27] for the treatment of electron correlations in extended systems. However, the computational effort is rather large so that applications are presently restricted to polymers. Localized Wannier orbitals provide an alternative to delocalized Bloch orbitals. Taking advantage of the exponential decay of Wannier orbitals for insulators and semiconductors, it is possible to perform HF [55] and correlated calculations [56] for extended systems with these orbitals.

The continuous spectrum of the HF Hamiltonian for Bloch orbitals requires an efficient computation of integrals in reciprocal space. These integrals are restricted to the first *Brillouin zone* (BZ) for semiconductors and to the region inside the Fermi surface for metals. Different types of quadrature schemes have been developed for metals, semiconductors and insulators [39, 44]. An alternative to quadrature schemes in reciprocal space are real space supercells. There exists a one-to-one correspondence between quadrature formulas in reciprocal space and real space supercells [16, 17, 40]. The supercell constitutes of a cluster of unit cells that is periodically extended into the whole space. Within this setting, the nonrelativistic supercell Hamiltonian [1] becomes

$$H_{SC} = \sum_{i=1}^{N} \left(-\frac{1}{2}\Delta_i + V_{\text{ext}}(\mathbf{r}_i) \right) + \sum_{\mathbf{R}} \sum_{i<j} \frac{1}{|\mathbf{r}_i - \mathbf{r}_j - \mathbf{R}|}, \tag{4}$$

where $\mathbf{R}$ are supercell lattice vectors, which map the original supercell into its periodic images. Only the N electrons assigned to the original supercell are treated explicitly and their interactions with electrons in other supercells are formally taken into account via the lattice sum in front of the Coulomb potential. It is however well known that this lattice sum does not converge and has to be replaced by an Ewald potential. Therefore, supercell Hamiltonians can be treated in electronic structure calculations almost like finite systems. The energy per supercell is given by the multiple integral

$$E_{SC} = \int_{SC} d^3r_1 \ldots \int_{SC} d^3r_N \, \Psi^*(\mathbf{r}_1, \ldots, \mathbf{r}_N) \, H_{SC} \, \Psi(\mathbf{r}_1, \ldots, \mathbf{r}_N), \tag{5}$$

with corresponding normalization condition for the wavefunction

$$\int_{SC} d^3r_1 \ldots \int_{SC} d^3r_N \, \Psi^*(\mathbf{r}_1, \ldots, \mathbf{r}_N) \Psi(\mathbf{r}_1, \ldots, \mathbf{r}_N) = 1. \tag{6}$$

We have adopted the supercell approach for two reasons. In our envisaged applications, we have to deal with excitons that are coupled to impurities or confined into quantum dots. Such kind of additional

[1] If not otherwise mentioned, atomic units have been used throughout this paper.

structures destroy the symmetry of the original primitive lattice. Therefore, the standard reciprocal space method is no longer applicable. Instead, the supercell approach provides a natural setting in this case, because of the local character of these additional structures in real space. For insulators and semiconductors with single impurities, the supercell approach became a standard method in solid state physics, see e.g. Refs. [15, 21, 35, 44]. The other reason is related to a possible extension of our method to correlated wavefunctions. In previous papers [18, 19, 36], we have discussed a product ansatz for wavelet approximations of correlated wavefunctions. This ansatz provides a sparse representation of electron correlations in real space, which can be efficiently exploited in the supercell approach. Furthermore, we can benefit from previous work within the QMC method, where the supercell approach has been extensively applied to jellium models and semiconductors [20].

It is decisive for practical applications to obtain fast convergence of the properties of a system with respect to the size of the supercell. Due to the one-to-one correspondence mentioned above, we can benefit in the supercell approach from optimized quadrature schemes in reciprocal space [15, 16]. Furthermore, the symmetry properties of many-electron wavefunctions [48, 49] can be exploited in order to improve convergence with respect to the supercell size. For metallic systems, however, the convergence is rather slow and in order to get rid of finite size errors it becomes necessary to extrapolate the results to an infinitely large supercell. Such kind of procedures have been extensively applied in QMC calculations for jellium models [20]. Despite its fundamental importance, we do not want to further pursue this subject in the present work. Instead, we are focusing on efficient and accurate numerical methods for solving the HF equation of a supercell with fixed size.

2.1 Basic definitions and notations for periodic systems

Before we can proceed with our discussion of the HF method, it is necessary to define a few basic quantities and to discuss some useful modifications of multiresolution analysis in the periodic supercell setting. We assume in the following that the system has an orthorhombic unit cell where the lattice vectors

$$\mathbf{A}_1 = (2^{u_1}, 0, 0)\,, \quad \mathbf{A}_2 = (0, 2^{u_2}, 0)\,, \quad \mathbf{A}_3 = (0, 0, 2^{u_3})\,, \tag{7}$$

are compatible with the underlying dyadic wavelet grid. According to standard conventions, we take reciprocal lattice vectors

$$\mathbf{B}_1 = 2\pi\left(2^{-u_1}, 0, 0\right), \quad \mathbf{B}_2 = 2\pi\left(0, 2^{-u_2}, 0\right), \quad \mathbf{B}_3 = 2\pi\left(0, 0, 2^{-u_3}\right). \tag{8}$$

Dyadic lattice vectors are mainly chosen for notational convenience and in more general cases it is possible to use different scaling factors along each direction of the lattice. The calculation of the Coulomb integrals requires only minor modifications in this case. Relaxing the constraint of orthogonal lattice vectors is more problematic and needs some fundamental modifications in the calculation of elementary one- and two-electron integrals. For our envisaged systems, however, this case seems to be of minor importance and we refrain from a further discussion of this topic. Another comment concerning our intended applications is appropriate at this place. In Section 1 we have mentioned several systems like jellium slabs, which require periodicity only in two dimensions. Nevertheless, we have based our approach on a three dimensional periodic lattice. Its is straightforward for such kind of systems to obtain an effective periodicity in two dimensions by choosing $|\mathbf{A}_1|$ sufficiently large compared to the thickness of the slab.

The supercell lattice vectors are defined as integer multiples of unit cell lattice vectors

$$\mathbf{D}_1 = N_1\mathbf{A}_1, \quad \mathbf{D}_2 = N_2\mathbf{A}_2, \quad \mathbf{D}_3 = N_3\mathbf{A}_3, \tag{9}$$

with length, sectional area and volume of the supercell given by

$$L_{SC} = N_1\, 2^{u_1}, \qquad A_{SC} = N_2 N_3\, 2^{u_2+u_3}, \qquad V_{SC} = L_{SC} A_{SC}. \tag{10}$$

For further usage, we also define translation vectors with respect to the supercell

$$\mathbf{R}_{\mathbf{n}} = \sum_i n_i \, \mathbf{D}_i, \quad n_i \in \mathbb{Z}, \tag{11}$$

and the corresponding wave vectors

$$\mathbf{k} = \sum_i \frac{n_i}{N_i} \mathbf{B}_i, \quad n_i \in \mathbb{Z}, \tag{12}$$

consistent with the reciprocal lattice of the supercell.

Two different types of tensor products can be used in order to obtain multivariate wavelets in $\mathbb{R}^3$ from an univariate wavelet basis in $\mathbb{R}$. In the first case, standard tensor products of univariate wavelets are used to define a multivariate wavelet basis. Within such kind of approach, combinations of wavelets on different levels occur and the tensor products have no well defined levels any more. These wavelet tensor products are therefore denoted as anisotropic wavelets. In the second case mixed tensor products of univariate wavelets and scaling functions on the same level are used to construct the multivariate wavelet basis. The resulting tensor products have well defined levels and are denoted as isotropic wavelets. Due to the quasi two-dimensional character of our systems, we use a mixture of both types of tensor products. Since we can expect that the HF orbitals behave rather uniform in the directions parallel to the slab, it is reasonable to use isotropic wavelets in these directions. In order to take into account the strongly anisotropic behaviour in the perpendicular direction, we have ultimately chosen anisotropic tensor products of univariate wavelets perpendicular to the slab with isotropic tensor products in the parallel directions. Further details concerning these tensor products, as well as some basic facts about wavelets can be found in Appendix A.

At next we want to adopt the wavelet basis to the periodic structure of the supercell. According to the tensor product ansatz for the multivariate wavelet basis it is obvious that we can limit our discussion to an univariate wavelet basis $\{\psi_{l,a_i}(x_i) : l, a_i \in \mathbb{Z}\}$ in the i'th direction. To each wavelet $\psi_{l,a}(x_i)$, we assign a lattice coordinate $2^{-l}a_i$ that specifies its location in real space. The set of wavelets $\{\psi_{l,a_i}(x_i) : a_i \in \mathbb{Z}\}$ on a fixed level l span a regular one dimensional lattice with lattice constant 2^{-l}. Depending on the specific size of the unit cell, we have to distinguish two cases. In the first case, the wavelet level l satisfies the inequality $l \geq -u_i$, which means that the distance between centers of neighbouring wavelets is smaller or equal to the unit cell size in the corresponding direction. Whereas in the second case, the reverse inequality $l < -u_i$ holds. Compatibility between supercell and wavelet lattice requires that only those wavelet levels l, which satisfy the consistency condition

$$2^{u_i+l} N_i \in \mathbb{N}, \tag{13}$$

can be used in the periodic setting. To get a standardized notation that comprises both cases, we introduce the integers

$$M_{l,i} := 2^{\min\{u_i+l,0\}} N_i, \tag{14}$$

and corresponding index sets

$$\Omega_{l,i} := \{n : 0 \leq n \leq M_{l,i} - 1\}. \tag{15}$$

Before we consider periodic wavelets, it is convenient to define a wavelet basis attached to the supercell. For this we introduce translation vectors within the supercell

$$\mathbf{t}_{l,\mathbf{n}} := \sum_i n_i \, 2^{-\min\{l+u_i,0\}} \, \mathbf{A}_i, \quad n_i \in \Omega_{l,i}, \tag{16}$$

and wave vectors

$$\boldsymbol{\kappa} := \sum_i \frac{n_i}{N_i} \mathbf{B}_i, \quad n_i \in \Omega_{l,i}, \tag{17}$$

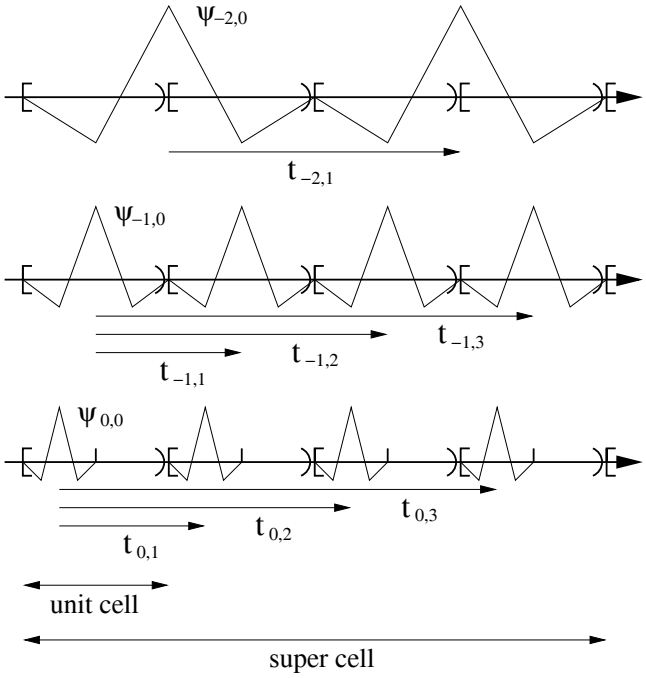

Figure 1: Supercell wavelets generated by linear combinations of wavelets within a supercell of size $N_i = 4$ and $u_i = 1$

.

restricted to the first BZ of the reciprocal lattice. By construction, these wave vectors reduce to the zero wave vector in the first BZ of the reciprocal supercell lattice. This condition can be modified in such a way that the wave vectors reduce to an arbitrary reference vector [16, 48, 49]. In the following, we adopt the notation that Greek characters denote momenta restricted to the first BZ, whereas Latin characters $\mathbf{k}$, $\mathbf{q}$ are used for unconstraint momenta (12). In the remaining part of this section, we again limit our discussion to one lattice direction. Since it is of no significance to specify the direction explicitly by denoting the index i for a specific component of vectors (16), (17) or index sets (14), (15), it is skipped in the following for the sake of notational simplicity. For example, instead of writing $t_{l,\mathbf{m},i}$ for the i'th component of the vector $\mathbf{t}_{l,\mathbf{m}}$, we use the shorthand notation $t_{l,m}$ in the following. We can now define univariate supercell wavelets

$$\psi_{l,c}^{\kappa}(x) := \frac{1}{\sqrt{M_l}} \sum_{m \in \Omega_l} e^{i\kappa t_{l,m}}\, \psi_{l,c}(x - t_{l,m}) = \frac{1}{\sqrt{M_l}} \sum_{m \in \Omega_l} e^{i\kappa t_{l,m}}\, \psi_{l,2^l t_{l,m}+c}(x), \tag{18}$$

for wave vectors κ through appropriate linear combinations of wavelets within the supercell. The translation parameters c of the supercell wavelets belong to the index set

$$\Lambda_l = \left\{ c : 0 \le c < 2^{\max\{u+l,0\}} \right\}, \tag{19}$$

which means that the lattice coordinate $2^{-l}c$ of the wavelet $\psi_{l,c}$ is within the first unit cell. This construction is schematically depicted in Fig. 1. For a biorthogonal wavelet basis, we can derive orthogonality relations between supercell wavelets and their dual counterparts

$$\int dx\, \psi_{j,a}^{\kappa'}(x)\, \tilde{\psi}_{l,b}^{\kappa *}(x) \;=\; \frac{1}{\sqrt{M_j M_l}} \sum_{p \in \Omega_j} \sum_{q \in \Omega_l} e^{i(\kappa' t_{j,p} - \kappa t_{l,q})} \int dx\, \psi_{j,2^j t_{j,p}+a}(x) \tilde{\psi}_{l,2^l t_{l,q}+b}(x)$$

$$
\begin{aligned}
&= \frac{\delta_{j,l}\,\delta_{a,b}}{M_j} \sum_{p\in\Omega_j} e^{i(\kappa'-\kappa)t_{j,p}} \\
&= \delta_{\kappa,\kappa'}\,\delta_{j,l}\,\delta_{a,b}.
\end{aligned} \tag{20}
$$

In the second line, we have used the orthogonality relation for biorthogonal wavelets (see Appendix A for details). For $j = l$, this lead us to the equation

$$
t_{j,p} - t_{j,q} = 2^{-j}(b-a), \tag{21}
$$

which can be only satisfied for $p = q$ and $a = b$, since by definition the left-hand side of Eq. (21) corresponds for $p \neq q$ to a shift from one unit cell to another. Obviously this is inconsistent with the definition of parameters a, b where we have assumed that the associated lattice coordinates are located in the first unit cell. The product between components of wave and translation vectors yields

$$
\begin{aligned}
(\kappa'-\kappa)t_{j,p} &= 2\pi\,\frac{n'-n}{N}\,2^{-\min\{j+u,0\}}\,p \\
&= 2\pi\,\frac{n'-n}{M_j}\,p,
\end{aligned} \tag{22}
$$

from which we immediately obtain the orthogonality relation (20).

Periodic wavelets are constructed by applying the periodic extension operator $\mathcal{R}$ to supercell wavelets

$$
\mathcal{R}\psi^{\kappa}_{l,c}(x) := \sum_{m\in\mathbb{Z}} \psi^{\kappa}_{l,c}(x - R_m) = \sum_{m\in\mathbb{Z}} \psi^{\kappa}_{l,2^l R_m + c}(x). \tag{23}
$$

If a reduction to a nonzero wave vector in the first BZ of the reciprocal supercell lattice is required [16, 48, 49], the definition (23) has to be modified by introducing an additional phase factor. Orthogonality relations for periodic wavelets are obtained with respect to dual supercell wavelets

$$
\int dx\,\mathcal{R}\psi^{\kappa'}_{j,a}(x)\,\tilde{\psi}^{\kappa *}_{l,b}(x) = \delta_{\kappa,\kappa'}\,\delta_{j,l}\,\delta_{a,b}. \tag{24}
$$

Further details concerning refinement relations for periodic wavelets are given Appendix B. Plane waves consistent with periodic boundary conditions can be conveniently expanded in the periodic wavelet basis

$$
\frac{1}{\sqrt{D}}\,e^{ikx} = \sum_j \sum_{a\in\Lambda_j} b^k_{j,a}\,\mathcal{R}\psi^{k|_j}_{j,a}(x), \tag{25}
$$

where the level dependent projection of a wave vector k into the first BZ is given by the common residue

$$
k|_j = k \bmod \left(\frac{2\pi M_j}{2^u N}\right). \tag{26}
$$

The periodic wavelet coefficients

$$
b^k_{j,a} = 2^{-\max\{j+u,0\}/2}\,e^{i\,2^{-j}ka}\,\hat{\tilde{\psi}}^{*}(2^{-j}k), \tag{27}
$$

can be directly evaluated using the Fourier transform of the dual mother wavelet $\hat{\tilde{\psi}}(\omega) := \int dx\,e^{-i\omega x}\tilde{\psi}(x)$.

3 Discrete Hartree-Fock equations for quasi two-dimensional systems

According to our envisaged applications, we have developed a discretization scheme for 3d-periodic HF equations, which is based on the assumption that the system is strongly inhomogeneous in one (perpendicular) direction and fairly homogeneous in the other two (parallel) directions. Within this scheme, we

define a decomposition of the periodic HF orbitals into local components $\phi_n^{\boldsymbol{\kappa}}(\mathbf{r})$ with compact support in a neighbourhood of the supercell. The periodic HF orbitals can be recovered by applying the periodic extension operator

$$\mathcal{R}\phi_n^{\boldsymbol{\kappa}}(\mathbf{r}) = \sum_{\mathbf{m}\in\mathbb{Z}^3} \phi_n^{\boldsymbol{\kappa}}(\mathbf{r}-\mathbf{R}_\mathbf{m}). \tag{28}$$

Due to the quasi two-dimensional character of the systems, we expect that the coupling between the perpendicular and parallel directions in the Hamiltonian remains rather weak. The local components are therefore expressed as linear combinations

$$\phi_n^{\boldsymbol{\kappa}}(\mathbf{r}) = \sum_{i=1}^{K} \left(\sum_\alpha C_{n,i,\alpha}^{\boldsymbol{\kappa}}\, \zeta_{\alpha,i}^{\boldsymbol{\kappa}}(\mathbf{r}) \right) \tag{29}$$

of tensor product functions

$$\zeta_{\alpha,i}^{\boldsymbol{\kappa}}(\mathbf{r}) = \psi_\alpha^{\kappa_1}(x)\Phi_i^{\boldsymbol{\kappa}_\parallel}(y,z), \tag{30}$$

where univariate supercell wavelets $\psi_\alpha^{\kappa_1}$ [2] are taken in the perpendicular direction and contracted isotropic supercell wavelets $\gamma_\alpha^{\boldsymbol{\kappa}_\parallel}$ in the parallel directions

$$\Phi_i^{\boldsymbol{\kappa}_\parallel}(y,z) = \sum_\alpha d_{i,\alpha}^{\boldsymbol{\kappa}_\parallel}\, \gamma_\alpha^{\boldsymbol{\kappa}_\parallel}(y,z). \tag{31}$$

It is reasonable to assume that the Kronecker rank K of the tensor product decomposition for the HF orbitals (29) can be kept small and almost independent of the size of the supercell through an appropriate choice of the contracted basis functions (31). In order to simplify the construction of the Fock matrix, a common set of basis functions in the parallel directions (31) has been chosen which does not depend on the perpendicular component κ_1 of the wave vector. Two possible approaches for these basis functions seem to be possible. In the first approach, the basis functions (31) are obtained from HF orbitals of the corresponding homogeneous system in either two or three dimensions. An even simpler choice would be a contraction of wavelets using plane waves or other appropriate systematic basis functions. The second approach consists in a self-consistent solution of the HF equations with respect to these parameters. According to the tensor product decomposition of the orbitals (29), this requires the treatment of a nonlinear optimization problem rather similar to the multi-configuration self-consistent field method.

From a computational point of view it is convenient to express expectation values with respect to the supercell in terms of local components (29) of the HF orbitals. This can be accomplished by introducing a finite version of the periodic extension operator

$$\mathcal{R}_M\phi_n^{\boldsymbol{\kappa}}(\mathbf{r}) := \sum_{\mathbf{m}\in\mathbb{M}^3} \phi_n^{\boldsymbol{\kappa}}(\mathbf{r}-\mathbf{R}_\mathbf{m}), \tag{32}$$

where $\mathbb{M}^3$ corresponds to a cube in $\mathbb{Z}^3$, centred at the origin, which contains M^3 lattice points. For HF orbitals, the normalization condition with respect to the supercell

$$\int_{V_{SC}} d^3r\, \mathcal{R}\phi_n^{\boldsymbol{\kappa}*}(\mathbf{r})\, \mathcal{R}\phi_{n'}^{\boldsymbol{\kappa}'}(\mathbf{r}) = \delta_{\boldsymbol{\kappa},\boldsymbol{\kappa}'}\delta_{n,n'} \tag{33}$$

can be expressed through unbounded integrals by considering an ensemble of supercells

$$\begin{aligned} \int_{V_{SC}} d^3r\, \mathcal{R}\phi_n^{\boldsymbol{\kappa}*}(\mathbf{r})\, \mathcal{R}\phi_{n'}^{\boldsymbol{\kappa}'}(\mathbf{r}) &= \frac{1}{M^3}\int_{\mathbb{R}^3} d^3r\, \mathcal{R}_M\phi_n^{\boldsymbol{\kappa}*}(\mathbf{r})\, \mathcal{R}_M\phi_{n'}^{\boldsymbol{\kappa}'}(\mathbf{r}) + O(M^{-1}) \\ &= \int_{\mathbb{R}^3} d^3r\, \phi_n^{\boldsymbol{\kappa}*}(\mathbf{r})\, \mathcal{R}_M\phi_{n'}^{\boldsymbol{\kappa}'}(\mathbf{r}) + O(M^{-1}). \end{aligned} \tag{34}$$

[2] In formulas where details concerning type, level and location of wavelets are not relevant, we use a single Greek wavelet index (ψ_α) to simplify our notation.

Replacing the periodic extension operator (28) by its finite variant (32), we approximate the supercell integral (33) by an average over a finite cube of supercells with surface error of $O(M^{-1})$. Taking the limit $M \to \infty$, we obtain an alternative version

$$\int_{\mathbb{R}^3} d^3r\, \phi_n^{\boldsymbol{\kappa}*}(\mathbf{r})\, \mathcal{R}\phi_{n'}^{\boldsymbol{\kappa}'}(\mathbf{r}) = \delta_{\boldsymbol{\kappa},\boldsymbol{\kappa}'}\delta_{n,n'} \tag{35}$$

of the normalization condition (33) in terms of unbounded integrals with respect to local components (29) of the HF orbitals.

The total HF energy can be split into a sum of one-particle, Coulomb and exchange contributions

$$E_{HF} = E_0 + E_c + E_x, \tag{36}$$

where we have to express each part in terms of local components (29) of the orbitals. This can be achieved using the same type of argument as for the normalization condition (35). The one-particle contribution becomes

$$\begin{aligned} E_0 &= 2\sum_{\boldsymbol{\kappa},n} \int_{V_{SC}} d^3r\, \mathcal{R}\phi_n^{\boldsymbol{\kappa}*}(\mathbf{r}) \left(-\frac{1}{2}\Delta + V_{\text{ext}}(\mathbf{r})\right) \mathcal{R}\phi_n^{\boldsymbol{\kappa}}(\mathbf{r}) \qquad (37)\\ &= \frac{2}{M^3}\sum_{\boldsymbol{\kappa},n} \int_{\mathbb{R}^3} d^3r\, \mathcal{R}_M\phi_n^{\boldsymbol{\kappa}*}(\mathbf{r}) \left(-\frac{1}{2}\Delta + V_{\text{ext}}(\mathbf{r})\right) \mathcal{R}_M\phi_n^{\boldsymbol{\kappa}}(\mathbf{r}) + O(M^{-1})\\ &= 2\sum_{\boldsymbol{\kappa},n} \int_{\mathbb{R}^3} d^3r\, \phi_n^{\boldsymbol{\kappa}*}(\mathbf{r}) \left(-\frac{1}{2}\Delta + V_{\text{ext}}(\mathbf{r})\right) \mathcal{R}_M\phi_n^{\boldsymbol{\kappa}}(\mathbf{r}) + O(M^{-1}), \qquad (38) \end{aligned}$$

where, in the second line, we have used the translational symmetry of the Hamiltonian. Analogous expressions can be obtained for the Coulomb

$$\begin{aligned} E_c &= 2\sum_{\boldsymbol{\kappa},\boldsymbol{\kappa}'}\sum_{n,n'} \int_{V_{SC}}\int_{V_{SC}} d^3r d^3r'\, \mathcal{R}\phi_n^{\boldsymbol{\kappa}*}(\mathbf{r})\, \mathcal{R}\phi_n^{\boldsymbol{\kappa}}(\mathbf{r})\, U_{\text{Ewald}}(\mathbf{r},\mathbf{r}')\, \mathcal{R}\phi_{n'}^{\boldsymbol{\kappa}'*}(\mathbf{r}')\, \mathcal{R}\phi_{n'}^{\boldsymbol{\kappa}'}(\mathbf{r}') \qquad (39)\\ &= \frac{2}{M^6}\sum_{\boldsymbol{\kappa},\boldsymbol{\kappa}'}\sum_{n,n'} \int_{\mathbb{R}^3}\int_{\mathbb{R}^3} d^3r d^3r'\, \mathcal{R}_M\phi_n^{\boldsymbol{\kappa}*}(\mathbf{r})\, \mathcal{R}_M\phi_n^{\boldsymbol{\kappa}}(\mathbf{r})\, U_{\text{Ewald}}(\mathbf{r},\mathbf{r}')\, \mathcal{R}_M\phi_{n'}^{\boldsymbol{\kappa}'*}(\mathbf{r}')\, \mathcal{R}_M\phi_{n'}^{\boldsymbol{\kappa}'}(\mathbf{r}') + O(M^{-1})\\ &= 2\sum_{\boldsymbol{\kappa},\boldsymbol{\kappa}'}\sum_{n,n'} \int_{\mathbb{R}^3}\int_{\mathbb{R}^3} d^3r d^3r'\, \phi_n^{\boldsymbol{\kappa}*}(\mathbf{r})\, \mathcal{R}_M\phi_n^{\boldsymbol{\kappa}}(\mathbf{r})\, U_{\text{Ewald}}(\mathbf{r},\mathbf{r}')\, \phi_{n'}^{\boldsymbol{\kappa}'*}(\mathbf{r}')\, \mathcal{R}_M\phi_{n'}^{\boldsymbol{\kappa}'}(\mathbf{r}') + O(M^{-1}), \end{aligned}$$

and exchange

$$\begin{aligned} E_x &= -\sum_{\boldsymbol{\kappa},\boldsymbol{\kappa}'}\sum_{n,n'} \int_{V_{SC}}\int_{V_{SC}} d^3r d^3r'\, \mathcal{R}\phi_{n'}^{\boldsymbol{\kappa}'*}(\mathbf{r})\, \mathcal{R}\phi_n^{\boldsymbol{\kappa}}(\mathbf{r})\, U_{\text{Ewald}}(\mathbf{r},\mathbf{r}')\, \mathcal{R}\phi_n^{\boldsymbol{\kappa}*}(\mathbf{r}')\, \mathcal{R}\phi_{n'}^{\boldsymbol{\kappa}'}(\mathbf{r}') \qquad (40)\\ &= -\sum_{\boldsymbol{\kappa},\boldsymbol{\kappa}'}\sum_{n,n'} \int_{\mathbb{R}^3}\int_{\mathbb{R}^3} d^3r d^3r'\, \phi_{n'}^{\boldsymbol{\kappa}'*}(\mathbf{r})\, \mathcal{R}_M\phi_n^{\boldsymbol{\kappa}}(\mathbf{r})\, U_{\text{Ewald}}(\mathbf{r},\mathbf{r}')\, \phi_n^{\boldsymbol{\kappa}*}(\mathbf{r}')\, \mathcal{R}_M\phi_{n'}^{\boldsymbol{\kappa}'}(\mathbf{r}') + O(M^{-1}) \end{aligned}$$

parts of the HF energy. Here we have already introduced an Ewald potential, which provides the necessary modification of the Coulomb interaction in order to get the two-electron integrals converged. The Ewald potential is discussed in more detail in Section 5. It only remains to perform the limit $M \to \infty$ to derive the final expressions for the HF expectation value of the energy

$$E_0 = 2\sum_{\boldsymbol{\kappa},n} \int_{\mathbb{R}^3} d^3r\, \phi_n^{\boldsymbol{\kappa}*}(\mathbf{r}) \left(-\frac{1}{2}\Delta + V_{\text{ext}}(\mathbf{r})\right) \mathcal{R}\phi_n^{\boldsymbol{\kappa}}(\mathbf{r}), \tag{41}$$

$$E_c = 2\sum_{\boldsymbol{\kappa},\boldsymbol{\kappa}'}\sum_{n,n'} \int_{\mathbb{R}^3}\int_{\mathbb{R}^3} d^3r d^3r'\, \phi_n^{\boldsymbol{\kappa}*}(\mathbf{r})\, \mathcal{R}\phi_n^{\boldsymbol{\kappa}}(\mathbf{r})\, U_{\text{Ewald}}(\mathbf{r},\mathbf{r}')\, \phi_{n'}^{\boldsymbol{\kappa}'*}(\mathbf{r}')\, \mathcal{R}\phi_{n'}^{\boldsymbol{\kappa}'}(\mathbf{r}'), \tag{42}$$

$$E_x = -\sum_{\boldsymbol{\kappa},\boldsymbol{\kappa}'}\sum_{n,n'}\int_{\mathbb{R}^3}\int_{\mathbb{R}^3} d^3r d^3r'\,\phi_{n'}^{\boldsymbol{\kappa}'*}(\mathbf{r})\,\mathcal{R}\phi_n^{\boldsymbol{\kappa}}(\mathbf{r})\,U_{\mathrm{Ewald}}(\mathbf{r},\mathbf{r}')\,\phi_n^{\boldsymbol{\kappa}*}(\mathbf{r}')\,\mathcal{R}\phi_{n'}^{\boldsymbol{\kappa}'}(\mathbf{r}'). \tag{43}$$

Variation of the HF energy (36) with respect to the orbital coefficients $C_{n,i,\alpha}^{\boldsymbol{\kappa}}$ yields the discrete closed shell HF equation

$$\sum_{j,\beta}\left[h_{ij,\alpha\beta}^{\boldsymbol{\kappa}} + 2J_{ij,\alpha\beta}^{\boldsymbol{\kappa}} - K_{ij,\alpha\beta}^{\boldsymbol{\kappa}}\right] C_{n,j,\beta}^{\boldsymbol{\kappa}} = \epsilon_n^{\boldsymbol{\kappa}} C_{n,i,\alpha}^{\boldsymbol{\kappa}}, \tag{44}$$

where the Fock matrix consists of one-particle

$$h_{ij,\alpha\beta}^{\boldsymbol{\kappa}} = \int_{\mathbb{R}^3} d^3r\,\zeta_{\alpha,i}^{\boldsymbol{\kappa}*}(\mathbf{r})\,\left(-\frac{1}{2}\Delta + V_{\mathrm{ext}}(\mathbf{r})\right)\,\mathcal{R}\zeta_{\beta,j}^{\boldsymbol{\kappa}}(\mathbf{r}), \tag{45}$$

Coulomb

$$J_{ij,\alpha\beta}^{\boldsymbol{\kappa}} = \sum_{\boldsymbol{\kappa}',n'}\int_{\mathbb{R}^3}\int_{\mathbb{R}^3} d^3r d^3r'\,\zeta_{\alpha,i}^{\boldsymbol{\kappa}*}(\mathbf{r})\,\mathcal{R}\zeta_{\beta,j}^{\boldsymbol{\kappa}}(\mathbf{r})\,U_{\mathrm{Ewald}}(\mathbf{r},\mathbf{r}')\,\phi_{n'}^{\boldsymbol{\kappa}'*}(\mathbf{r}')\,\mathcal{R}\phi_{n'}^{\boldsymbol{\kappa}'}(\mathbf{r}'), \tag{46}$$

and exchange

$$K_{ij,\alpha\beta}^{\boldsymbol{\kappa}} = \sum_{\boldsymbol{\kappa}',n'}\int_{\mathbb{R}^3}\int_{\mathbb{R}^3} d^3r d^3r'\,\zeta_{\alpha,i}^{\boldsymbol{\kappa}*}(\mathbf{r})\,\mathcal{R}\phi_{n'}^{\boldsymbol{\kappa}'}(\mathbf{r})\,U_{\mathrm{Ewald}}(\mathbf{r},\mathbf{r}')\,\phi_{n'}^{\boldsymbol{\kappa}'*}(\mathbf{r}')\,\mathcal{R}\zeta_{\beta,j}^{\boldsymbol{\kappa}}(\mathbf{r}'). \tag{47}$$

matrices. The strongly anisotropic character of these equations is expressed through the double indices α, i where we assume $\mathrm{card}\{\alpha\} \gg \mathrm{card}\{i\}$ for the cardinalities of the corresponding index sets.

4 Construction of the Fock matrix

From a formal point of view our treatment of the HF method is completely standard and the only multiscale feature that has entered into our discussion so far is the tensor product decomposition of the orbitals (29). At next we want to discuss some applications of multiresolution analysis to the construction of the Fock matrix, which is the time determining step for the solution of the discrete HF equations (44). Coulomb and exchange matrices can be computed in an efficient way using sparse nonstandard representations of Ewald potentials in the wavelet basis. Concerning a detailed discussion of certain sparsity properties related to Ewald potentials, we refer to Section 6 below. The nonstandard representation of integral operators has been introduced into multiresolution analysis by Beylkin, Coifman and Rokhlin [7, 8]. A typical feature of this representation is that couplings between wavelets on different levels are replaced by couplings between wavelets and scaling functions on the same level. It provides an efficient scheme for the calculation of two-electron integrals, which has been discussed in detail in Ref. [18]. Due to the relatively small number of degrees of freedom in the parallel directions, we advocate a two-step procedure. The first step involves the construction of intermediate nonstandard Coulomb

$${}^{(p,q)}J_{stuv,j,a}^{\boldsymbol{\kappa}_\parallel\boldsymbol{\kappa}'_\parallel} = \int_{\mathbb{R}^3}\int_{\mathbb{R}^3} d^3r d^3r'\,\psi_{j,a}^{(p)}(x)\,\Phi_s^{\boldsymbol{\kappa}'_\parallel *}(\mathbf{r}_\parallel)\,\mathcal{R}\Phi_t^{\boldsymbol{\kappa}'_\parallel}(\mathbf{r}_\parallel)\,U_{\mathrm{Ewald}}(\mathbf{r},\mathbf{r}')\,\Phi_u^{\boldsymbol{\kappa}_\parallel *}(\mathbf{r}'_\parallel)\,\mathcal{R}\Phi_v^{\boldsymbol{\kappa}_\parallel}(\mathbf{r}'_\parallel)\,\psi_{j,0}^{(q)}(x'), \tag{48}$$

and exchange integrals

$${}^{(p,q)}K_{stuv,j,a}^{\boldsymbol{\kappa}_\parallel\boldsymbol{\kappa}'_\parallel} = \int_{\mathbb{R}^3}\int_{\mathbb{R}^3} d^3r d^3r'\,\psi_{j,a}^{(p)}(x)\,\Phi_s^{\boldsymbol{\kappa}'_\parallel *}(\mathbf{r}_\parallel)\,\mathcal{R}\Phi_t^{\boldsymbol{\kappa}_\parallel}(\mathbf{r}_\parallel)\,U_{\mathrm{Ewald}}(\mathbf{r},\mathbf{r}')\,\Phi_u^{\boldsymbol{\kappa}_\parallel *}(\mathbf{r}'_\parallel)\,\mathcal{R}\Phi_v^{\boldsymbol{\kappa}'_\parallel}(\mathbf{r}'_\parallel)\,\psi_{j,0}^{(q)}(x'), \tag{49}$$

which remain fixed during the self-consistent solution of the HF equation. We demonstrate in Section 6 below, that these integrals are sparse with respect to the index a, due to the vanishing moment property of the wavelet basis. It should be noticed that within the nonstandard scheme, pure scaling function integrals ($p = q = 0$) are required on the coarsest level only.

For the calculation of intermediate Coulomb and exchange integrals, we have to expand products of basis functions in the parallel directions within the wavelet basis. Such kind of expansion requires wavelet coupling coefficients between supercell and periodic wavelets

$$\eta_{\alpha,\beta,\mu}^{\boldsymbol{\kappa}_\parallel,\boldsymbol{\kappa}'_\parallel} := \int_{\mathbb{R}^2} d^2 r_\parallel \, \gamma_\alpha^{\boldsymbol{\kappa}_\parallel *}(\mathbf{r}_\parallel) \, \mathcal{R}\gamma_\beta^{\boldsymbol{\kappa}'_\parallel}(\mathbf{r}_\parallel) \, \tilde{\gamma}_\mu(\mathbf{r}_\parallel), \tag{50}$$

and sums involving contraction coefficients (31)

$$\eta_{st,\mu}^{\boldsymbol{\kappa}_\parallel,\boldsymbol{\kappa}'_\parallel} := \sum_{\alpha,\beta} d_{s,\alpha}^{\boldsymbol{\kappa}_\parallel *} \, d_{t,\beta}^{\boldsymbol{\kappa}'_\parallel} \, \eta_{\alpha,\beta,\mu}^{\boldsymbol{\kappa}_\parallel,\boldsymbol{\kappa}'_\parallel}. \tag{51}$$

Computation of wavelet coupling coefficients and their properties has been described in detail in Ref. [18]. With these coefficients at hand, the wavelet expansion of a product of basis functions is given by

$$\Phi_s^{\boldsymbol{\kappa}_\parallel *}(\mathbf{r}_\parallel) \, \mathcal{R}\Phi_t^{\boldsymbol{\kappa}'_\parallel}(\mathbf{r}_\parallel) = \sum_\alpha \eta_{st,\alpha}^{\boldsymbol{\kappa}_\parallel,\boldsymbol{\kappa}'_\parallel} \, \gamma_\alpha(\mathbf{r}_\parallel). \tag{52}$$

The Ewald potential can be represented in the nonstandard form

$$U_{\mathrm{Ewald}}(\mathbf{r}_1,\mathbf{r}_2) = \sum_{j=j_0}^{j\mathrm{max}} {\sum_{p,q}}' \sum_{\mathbf{a},\mathbf{b}} \langle \gamma_{j,\mathbf{a}}^{(p)} | U_{\mathrm{Ewald}} | \gamma_{j,\mathbf{b}}^{(q)} \rangle \, \tilde{\gamma}_{j,\mathbf{a}}^{(p)}(\mathbf{r}_1) \, \tilde{\gamma}_{j,\mathbf{b}}^{(q)}(\mathbf{r}_2), \tag{53}$$

where the wavelet matrix elements of the Ewald potential are given by

$$\langle \gamma_{j,\mathbf{a}}^{(p)} | U_{\mathrm{Ewald}} | \gamma_{j,\mathbf{b}}^{(q)} \rangle = \int_{\mathbb{R}^3} \int_{\mathbb{R}^3} d^3 r_1 d^3 r_2 \, \gamma_{j,\mathbf{a}}^{(p)}(\mathbf{r}_1) \, U_{\mathrm{Ewald}}(\mathbf{r}_1,\mathbf{r}_2) \, \gamma_{j,\mathbf{b}}^{(q)}(\mathbf{r}_2). \tag{54}$$

A prime at the sum over p, q indicates that pure scaling function matrix elements contribute on the coarsest level only. We use the same symbol γ for isotropic 2d and 3d wavelets. The latter are given by tensor products of univariate and isotropic 2d wavelets, i.e.

$$\gamma_{j,\mathbf{a}}^{(p)}(\mathbf{r}) = \psi_{j,a_1}^{(p_1)}(x) \, \gamma_{j,\mathbf{a}_\parallel}^{(p_\parallel)}(\mathbf{r}_\parallel), \tag{55}$$

with obvious relations between the parameters p and $p_1, p_\parallel$ characterizing the wavelet types on both sides of the equation, see Appendix A for further details. Inserting the wavelet expansion (53) into the integrals (48) and (49), reveals after some algebraic manipulations, the following expressions for intermediate Coulomb

$${}^{(p_1,q_1)}J_{stuv,j,a_1}^{\boldsymbol{\kappa}_\parallel\boldsymbol{\kappa}'_\parallel} = {}^{(p_1,q_1)}\bar{J}_{stuv,j,a_1}^{\boldsymbol{\kappa}_\parallel\boldsymbol{\kappa}'_\parallel} + \sum_{n=1}^{j_{max}} {}^{(p_1,q_1)}H_{b-2^n a_1}^{n\ (0,0)} \bar{J}_{stuv,j+n,b}^{\boldsymbol{\kappa}_\parallel\boldsymbol{\kappa}'_\parallel}, \tag{56}$$

and exchange integrals

$${}^{(p_1,q_1)}K_{stuv,j,a_1}^{\boldsymbol{\kappa}_\parallel\boldsymbol{\kappa}'_\parallel} = {}^{(p_1,q_1)}\bar{K}_{stuv,j,a_1}^{\boldsymbol{\kappa}_\parallel\boldsymbol{\kappa}'_\parallel} + \sum_{n=1}^{j_{max}} {}^{(p_1,q_1)}H_{b-2^n a_1}^{n\ (0,0)} \bar{K}_{stuv,j+n,b}^{\boldsymbol{\kappa}_\parallel\boldsymbol{\kappa}'_\parallel}, \tag{57}$$

where the individual terms

$${}^{(p_1,q_1)}\bar{J}_{stuv,j,a_1}^{\boldsymbol{\kappa}_\parallel\boldsymbol{\kappa}'_\parallel} = {\sum_{p_\parallel,q_\parallel}}' \sum_{\mathbf{a}_\parallel} \left[\sum_{\mathbf{b}_\parallel} \eta_{st,j,p_\parallel,\mathbf{a}_\parallel+\mathbf{b}_\parallel}^{\boldsymbol{\kappa}'_\parallel,\boldsymbol{\kappa}'_\parallel} \, \eta_{uv,j,q_\parallel,\mathbf{b}_\parallel}^{\boldsymbol{\kappa}_\parallel,\boldsymbol{\kappa}_\parallel} \right] \langle \gamma_{j,\mathbf{a}}^{(p)} | U_{\mathrm{Ewald}} | \gamma_{j,\mathbf{0}}^{(q)} \rangle, \tag{58}$$

$$ {}^{(p_1,q_1)}\bar{K}^{\boldsymbol{\kappa}_\parallel \boldsymbol{\kappa}'_\parallel}_{stuv,j,a_1} = {\sum_{p_\parallel,q_\parallel}}' \sum_{\mathbf{a}_\parallel} \left[\sum_{\mathbf{b}_\parallel} \eta^{\boldsymbol{\kappa}'_\parallel,\boldsymbol{\kappa}_\parallel}_{st,j,p_\parallel,\mathbf{a}_\parallel+\mathbf{b}_\parallel} \eta^{\boldsymbol{\kappa}_\parallel,\boldsymbol{\kappa}'_\parallel}_{uv,j,q_\parallel,\mathbf{b}_\parallel} \right] \langle \gamma^{(p)}_{j,\mathbf{a}} | U_{\mathrm{Ewald}} | \gamma^{(q)}_{j,\mathbf{0}} \rangle, \tag{59} $$

correspond to sums with contributions from the same level only. The derivation of expressions (56) and (57) uses the biorthogonality of the wavelet basis and multiscale relations for bilinear forms of univariate wavelets, see Appendix A for further details.

In each iteration of the self-consistent solution of the HF equation, the Fock matrix has to be constructed from intermediate Coulomb (48) and exchange (49) integrals. This requires the evaluation of univariate wavelet coupling coefficients in the perpendicular direction

$$ \eta^{\kappa\kappa'}_{\alpha,\beta,\nu} := \int dx\, \psi^{\kappa *}_{\alpha}(x)\, \mathcal{R}\psi^{\kappa'}_{\beta}(x)\, \tilde{\psi}_{\nu}(x), \tag{60} $$

and their contractions with orbital coefficients

$$ \eta^{\boldsymbol{\kappa}'\kappa_1}_{n',u,\beta,\nu} := \sum_{\alpha} C^{\boldsymbol{\kappa}'*}_{n',u,\alpha}\, \eta^{\kappa'_1\kappa_1}_{\alpha,\beta,\nu}, \qquad \eta^{\kappa_1\boldsymbol{\kappa}'}_{n',u,\alpha,\nu} := \sum_{\beta} C^{\boldsymbol{\kappa}'}_{n',u,\beta}\, \eta^{\kappa_1\kappa'_1}_{\alpha,\beta,\nu}, \qquad \eta^{\boldsymbol{\kappa}'\boldsymbol{\kappa}'}_{n',uv,\nu} := \sum_{\alpha} C^{\boldsymbol{\kappa}'*}_{n',u,\alpha}\, \eta^{\kappa'_1\boldsymbol{\kappa}'}_{n',v,\alpha,\nu}. \tag{61} $$

The computational complexity for the evaluation of the coefficients (60) and (61) can be estimated with respect to size of the univariate wavelet basis within a unit cell. It should be emphasized that we take a given supercell with a fixed number of electrons and consider the computational complexity with respect to a refinement of the wavelet basis. Within a unit cell, the cardinality of the univariate wavelet basis

$$ \mathrm{card}\{\psi_\alpha\} = O(L), \text{ with } \; L = 2^{j_{max}}, \tag{62} $$

increases exponentially with the finest wavelet level j_{max}. Straightforward combinatorial arguments [19], based on the hierarchical structure and compact supports of wavelets, show that the cardinality of wavelet coupling coefficients (60)

$$ \mathrm{card}\{\eta^{\kappa\kappa'}_{\alpha,\beta,\nu}\} = O\left(L \log(L)^2\right), \tag{63} $$

increases almost linear with the number of univariate wavelets in a unit cell. The estimated cardinalities of the contracted coefficients (61)

$$ \mathrm{card}\{\eta^{\kappa_1\boldsymbol{\kappa}'}_{n',u,\alpha,\nu}\} = O\left(K\, L \log(L)\right), \tag{64} $$

$$ \mathrm{card}\{\eta^{\boldsymbol{\kappa}'\boldsymbol{\kappa}'}_{n',uv,\nu}\} = O\left(K^2\, L\right), \tag{65} $$

also depend on the Kronecker rank K, which is assumed to be small i.e. $K \ll L$. It is possible to calculate these coefficients with $O\left(K^2\, L \log(L)^2\right)$ computational complexity.

For the evaluation of Coulomb

$$ J^{\boldsymbol{\kappa}}_{st,\alpha\beta} = \sum_{\boldsymbol{\kappa}',n'} \sum_{u,v} \sum_{m} {\sum_{p_1,q_1}}' \sum_{c} \left[\sum_{d} \eta^{\boldsymbol{\kappa}'\boldsymbol{\kappa}'}_{n',uv,m,p_1,c+d}\, \eta^{\kappa_1\kappa_1}_{\alpha,\beta,m,q_1,d} \right] {}^{(p_1,q_1)}J^{\boldsymbol{\kappa}'_\parallel \boldsymbol{\kappa}_\parallel}_{stuv,m,c}, \tag{66} $$

and exchange

$$ K^{\boldsymbol{\kappa}}_{st,\alpha\beta} = \sum_{\boldsymbol{\kappa}',n'} \sum_{u,v} \sum_{m} {\sum_{p_1,q_1}}' \sum_{c} \left[\sum_{d} \eta^{\kappa_1\boldsymbol{\kappa}'}_{n',u,\alpha,m,p_1,c+d}\, \eta^{\boldsymbol{\kappa}'\kappa_1}_{n',v,\beta,m,q_1,d} \right] {}^{(p_1,q_1)}K^{\boldsymbol{\kappa}_\parallel \boldsymbol{\kappa}'_\parallel}_{suvt,m,c}, \tag{67} $$

matrix elements further contractions of the coefficients (60) and (61) are required. In order to estimate the computational complexity of the Fock matrix, we have assumed that the intermediate Coulomb and exchange integrals (48) and (49) are sparse. Focusing on the sums in the square brackets, we obtain computational complexities of $O\left(K^4 L \log(L)^2\right)$ and $O\left(K^4\, L^2\right)$ for Coulomb and exchange matrix elements, respectively. The L^2 dependence of the exchange matrix elements is deminished by the exponential decay of the exchange interaction, which has not been taken into account by our formal arguments. This topic is further discussed in Section 6.

5 Wavelet representation of Ewald potentials

A standard approach to electronic structure calculations for periodic systems [20, 55] is to replace the Coulomb interaction in the Hamiltonian (4) by an Ewald potential

$$U_{\mathrm{Ewald}}(\mathbf{r}_i,\mathbf{r}_j)=\sum_{\mathbf{R}}\frac{\mathrm{erfc}(\sqrt{\lambda}|\mathbf{r}_i-\mathbf{r}_j-\mathbf{R}|)}{|\mathbf{r}_i-\mathbf{r}_j-\mathbf{R}|}+\frac{4\pi}{V_{SZ}}\sum_{\mathbf{k}\neq 0}\frac{1}{|\mathbf{k}|^2}e^{-\frac{\mathbf{k}^2}{4\lambda}+i\mathbf{k}(\mathbf{r}_i-\mathbf{r}_j)}-\frac{\pi}{\lambda V_{SZ}}, \tag{68}$$

which takes into account the Coulomb interaction between an electron located at $\mathbf{r}_i$ and another electron at $\mathbf{r}_j$ as well as with all the mirror images of the second electron located at $\mathbf{r}_j+\mathbf{R}$ in other supercells. In order to make this sum converge, the interaction with a homogeneous background charge-density has to be subtracted resulting in the Ewald potential (68). The parameter $\lambda>0$ can be adjusted to get a balanced convergence of the real and reciprocal lattice sums. For the evaluation of elementary two-electron integrals (54), we can rely on techniques originally developed for the Coulomb interaction in Ref. [18]. First we observe, that due to the presence of absolute length-scales $|\mathbf{D}_i|$ cf. Eq. (11), no simple scaling relation between different wavelet levels exists. Consequently, we cannot directly apply the iterative scheme of Beylkin, Dahmen and Micchelli as outlined in Ref. [18] for the Coulomb interaction. However, it is straightforward to adapt the Gaussian transform method to the first term in the Ewald potential. By a simple change of the integration variable, we obtain the integral representation

$$\frac{\mathrm{erfc}(\sqrt{\lambda}|\mathbf{r}_1-\mathbf{r}_2-\mathbf{R}|)}{|\mathbf{r}_1-\mathbf{r}_2-\mathbf{R}|}=\frac{2}{\sqrt{\pi}}\int_{\sqrt{\lambda}}^{\infty}dt\,e^{-t^2|\mathbf{r}_1-\mathbf{r}_2-\mathbf{R}|^2}. \tag{69}$$

This means that we can apply the Gaussian transform method described in Ref. [18] by changing the integration interval for the auxilliary variable t from $[0,\infty)$ to $[\sqrt{\lambda},\infty)$. Analogously to Ref. [18], we introduce the functions

$$G_{\mathrm{Ewald}}(j,a_i,t)=2^{-j}\sum_{R_i}\int_{\mathbb{R}}\int_{\mathbb{R}}dx_1dx_2\,\varphi(x_1-a_i+2^jR_i)\,e^{-(x_1-x_2)^2 2^{-2j}t^2}\,\varphi(x_2), \tag{70}$$

where the lattice sum factorizes into sums for single components R_i of the supercell vectors.

Once we have obtained the integrals for scaling functions on level j, refinement relations can be applied in order to get the corresponding wavelet integrals on level $j-1$. There is however a simple alternative to compute wavelet integrals (p or $q\neq 0$) by means of the direct sum

$$\langle\gamma^{(p)}_{j,\mathbf{a}}|U_{\mathrm{Ewald}}|\gamma^{(q)}_{j,\mathbf{0}}\rangle=\sum_{\mathbf{R}}\int_{\mathbb{R}^3}\int_{\mathbb{R}^3}d^3r_1d^3r_2\,\gamma^{(p)}_{j,\mathbf{a}}(\mathbf{r}_1)\,\frac{1}{|\mathbf{r}_1-\mathbf{r}_2-\mathbf{R}|}\gamma^{(q)}_{j,\mathbf{0}}(\mathbf{r}_2). \tag{71}$$

For wavelet integrals, the constant term in the Ewald potential (68) vanishes. This is due to the vanishing moment property of wavelets. Therefore it is possible to take $\lim\lambda\to 0$ for these integrals. In this limit, the wavelet integral of the Ewald potential (54) is equivalent to the direct sum (71).

An interesting observation can be made for a specific choice of the coarsest level j_0 in the wavelet basis, where only a single grid point $\mathbf{a}=\mathbf{0}$ remains in the supercell. For this case, all integrals (54) involving scaling functions on the coarsest level exactly vanish

$$\langle\gamma^{(p)}_{j_0,\mathbf{0}}|U_{\mathrm{Ewald}}|\gamma^{(0)}_{j_0,\mathbf{0}}\rangle=0,\ \text{if}\ \ 2^{j_0+u_i}N_i=1. \tag{72}$$

In order to proof this statement, we first consider the function (70) for this specific choice of the parameters

$$\begin{aligned}G_{\mathrm{Ewald}}(j_0,0,t) &= 2^{-j_0}\sum_{n\in\mathbb{Z}}\int_{\mathbb{R}}\int_{\mathbb{R}}dx_1dx_2\,\psi^{(0)}(x_1+n)\,e^{-(x_1-x_2)^2 2^{-2j_0}t^2}\,\psi^{(p)}(x_2)\\ &= 2^{-j_0}\int_{\mathbb{R}}\int_{\mathbb{R}}dx_1dx_2\,e^{-(x_1-x_2)^2 2^{-2j_0}t^2}\,\psi^{(p)}(x_2)\\ &= \frac{\sqrt{\pi}}{t}\,\delta_{0,p},\end{aligned} \tag{73}$$

where we have used the partition of unity $1 = \sum_a \varphi(x+a)$, which applies for all kinds of scaling functions. The integral with respect to the first term in the Ewald potential (68), therefore, becomes

$$\begin{aligned}\int_{\mathbb{R}^3}\int_{\mathbb{R}^3} d^3r_1 d^3r_2\, \gamma^{(p)}_{j_0,\mathbf{0}}(\mathbf{r}_1) \sum_{\mathbf{R}} \frac{\operatorname{erfc}(\sqrt{\lambda}|\mathbf{r}_1-\mathbf{r}_2-\mathbf{R}|)}{|\mathbf{r}_1-\mathbf{r}_2-\mathbf{R}|}\, \gamma^{(0)}_{j_0,\mathbf{0}}(\mathbf{r}_2) &= 2\pi\delta_{0,p}\int_{\sqrt{\lambda}}^{\infty} dt\, \frac{1}{t^3} \\ &= \frac{\pi}{\lambda}\delta_{0,p}, \end{aligned} \tag{74}$$

which exactly cancels the contribution of the third term to the integral, since by definition we have $V_{SC} = 2^{-3j_0}$. A simple calculation for the Fourier integrals appearing in the reciprocal lattice sum

$$\begin{aligned}\int_{\mathbb{R}} dx\, e^{i2^{-j_0}kx}\psi^{(0)}(x) &= \sum_{a\in\mathbb{Z}}\int_0^1 dx\, e^{i2^{-j_0}kx}\psi^{(0)}(x-a) \\ &= \int_0^1 dx\, e^{i2\pi nx} \\ &= 0, \text{ if } k = 2^{j_0}2\pi n \neq 0, \end{aligned} \tag{75}$$

demonstrates that the second term also vanishes. The simple physical reason behind Eq. (72) is that the only function, consistent with periodic boundary conditions, which can be represented by scaling functions on level j_0 is the constant function. By definition of the Ewald potential, however, the interaction energy between an arbitrary and a constant charge distribution vanishes.

6 Multiresolution Hartree-Fock for jellium slabs

An essential feature of wavelet expansions is their sparsity due to the vanishing moment property. Within this section, we want to discuss some sparsity properties of intermediate Coulomb (48) and exchange (49) integrals. For this it is necessary to study the asymptotic smoothness of the corresponding kernel functions, which is conveniently done for jellium slabs, where orbital contributions in the parallel directions are known explicitly. The HF orbitals factorize into simple products

$$\mathcal{R}\phi_n^{\mathbf{k}_\parallel}(\mathbf{r}) = \mathcal{R}\xi_n^{\mathbf{k}_\parallel}(x)\, \frac{1}{\sqrt{A_{SC}}}\, e^{i\mathbf{k}_\parallel \mathbf{r}_\parallel}, \tag{76}$$

where the parallel directions correspond to plane waves. According to our tensor product ansatz (29), we take a wavelet expansion

$$\xi_n^{\mathbf{k}_\parallel}(x) = \sum_\alpha C^{\mathbf{k}_\parallel}_{n,\alpha}\, \psi_\alpha(x) \tag{77}$$

for the perpendicular part of the orbitals. Within our approach, we consider a supercell of the form shown in Fig. 2 with unit cells extending over the whole width of the supercell in the direction perpendicular to the slab. Furthermore it is required that the width of the slab is small compared to the size of the supercell i.e. $S \ll D_1$. As a consequence, we can assume that the perpendicular parts of the orbitals $\xi_n^{\mathbf{k}_\parallel}(x)$ have compact supports within the supercell and belong to momentum $k_1 = 0$. The remaining dependence on momenta parallel to the slab is due to the nonlocal exchange operator present in the HF equations. For this reason, there have been no exact HF calculations for jellium surfaces or slabs reported in the literature. However, numerous approximate HF calculations, following the pioneering work of Bardeen [5], have been published see e.g. [23, 37, 51, 52, 53, 54]. Within these calculations, the nonlocal exchange operator was approximated by a local potential. As a consequence, the perpendicular part $\xi_n(x)$ does no longer depend on the momenta in the parallel directions, which greatly simplifies the numerical treatment. The same type of argument applies to DFT, where only local potentials appear in the Kohn-Sham equation.

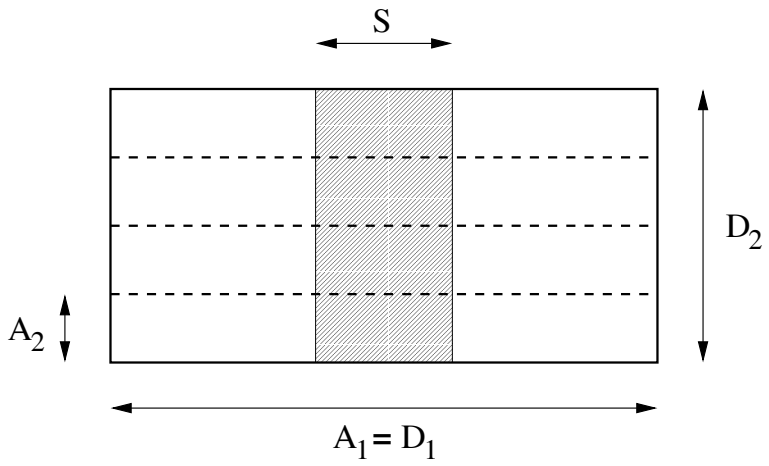

Figure 2: Supercell for a jellium slab

After these introductory remarks, we want to consider intermediate Coulomb integrals (48) for jellium slabs. It is straightforward in this case to integrate out the parallel directions analytically. The Fourier representation of the Ewald potential leads to an effective Coulomb potential

$$\begin{aligned} U_J(x,x') &= \frac{1}{A_{SC}^2}\int_{A_{SC}}\int_{A_{SC}} dr_\parallel^2\, dr_\parallel'^2\, U_{\mathrm{Ewald}}(\mathbf{r},\mathbf{r}') \\ &= \frac{4\pi}{V_{SC}}\sum_{k_1\neq 0}\frac{e^{ik_1(x-x')}}{k_1^2}, \end{aligned} \tag{78}$$

which can be expressed through a reciprocal lattice sum in the perpendicular direction. Taking a wavelet representation of this potential, we can identify the corresponding integrals with intermediate Coulomb integrals (48)

$$\begin{aligned} {}^{(s,t)}J_{j,a} &= \int_{\mathbb{R}}\int_{\mathbb{R}} dx\, dx'\, \psi_{j,a}^{(s)}(x)\, U_J(x,x')\, \psi_{j,0}^{(t)}(x') \\ &= \frac{4\pi}{V_{SC}}\, 2^{-j}\sum_{q_1\neq 0}\frac{e^{ia2^{-j}q_1}}{q_1^2}\,\hat{\psi}^{(s)}(2^{-j}q_1)^*\,\hat{\psi}^{(t)}(2^{-j}q_1). \end{aligned} \tag{79}$$

In order to study the analytic behaviour of the effective Coulomb potential (78) near the diagonal, we have introduced an infrared cutoff parameter ϵ and performed the transition to the continuum limit

$$\begin{aligned} U_J(x,x') &\sim \frac{2}{A_{SC}}\left[\int_{-\infty}^{-\epsilon} dk_1\,\frac{e^{ik_1(x-x')}}{k_1^2} + \int_{\epsilon}^{\infty} dk_1\,\frac{e^{ik_1(x-x')}}{k_1^2}\right] \\ &= \frac{4}{A_{SC}}\left[\frac{\cos\left(\epsilon(x-x')\right)}{\epsilon} + (x-x')\,\mathrm{Si}\left(\epsilon(x-x')\right) - \frac{\pi}{2}|x-x'|\right], \end{aligned} \tag{80}$$

where the sum has been replaced by an integral. For our following considerations it is not essential to specify the parameter ϵ. However, it seems to be convenient to require coincidence of the effective potential (78) and its asymptotic expansion (80) along the diagonal. A simple computation using Eq. (78) yields

$$U_J(x,x) = \frac{\pi L_{SC}^2}{3V_{SC}}, \tag{81}$$

from which we obtain, together with Eq. (80), the condition

$$\epsilon = \frac{12}{\pi L_{SC}}. \tag{82}$$

It should be emphasized that Eq. (80) is only valid asymptotically near the diagonal and does not yield the correct continuum limit of the effective potential (78). The infrared cutoff introduces some arbitraryness in the long-range behaviour, which cannot be cured by an appropriate choice of the parameter ϵ. This limitation, however, does not affect our considerations, which just rely on the properties of the effective potential near the diagonal. It follows immediately from the Taylor series of the cosine and integral sine that the first two terms in the asymptotic formula (80) contain only even powers of $|x-x'|$. Therefore it is the linear $|x-x'|$ term which determines the regularity of the effective potential and hence the sparsity of the intermediate Coulomb integrals (48). Pure scaling function integrals (79) are well approximated by the asymptotic formula (80), as can be seen in Fig. 3 a) for different size of the supercell. This is due to the interpolation property of our scaling functions. For intermediate Coulomb integrals involving wavelets, a very fast decay can be observed beyond a certain characteristic value of the translation parameter a, which is shown in Fig. 3 b). Beyond this characteristic value, the supports of the wavelets or scaling functions in the integrand do not overlap anymore. Therefore, the diagonal cusp of the effective potential does not contribute to the integrals.

Exchange potentials for jellium slabs can be treated along the same line as the Coulomb potential. The kernel function of the effective exchange potential in the perpendicular direction

$$\begin{aligned} U_K^{\mathbf{k}_\parallel \mathbf{k}'_\parallel}(x,x') &= \frac{1}{A_{SC}^2} \int_{A_{SC}} \int_{A_{SC}} dr_\parallel^2 \, dr_\parallel'^2 \, e^{-i(\mathbf{k}'_\parallel - \mathbf{k}_\parallel)\mathbf{r}_\parallel} \, U_{\mathrm{Ewald}}(\mathbf{r},\mathbf{r}') \, e^{i(\mathbf{k}'_\parallel - \mathbf{k}_\parallel)\mathbf{r}'_\parallel} \\ &= \frac{4\pi}{V_{SC}} \sum_{k_1}{}' \frac{e^{ik_1(x-x')}}{k_1^2 + |\mathbf{k}_\parallel - \mathbf{k}'_\parallel|^2}, \end{aligned} \tag{83}$$

however, depends on the momenta parallel to the slab. A prime at the reciprocal lattice sum indicates that it restricts to those values of k_1 for which the denominator does not vanish. Again, intermediate exchange integrals (49) correspond to integrals of the wavelet representation of the kernel function (83)

$$\begin{aligned} {}^{(s,t)}K_{j,a}^{\mathbf{k}_\parallel \mathbf{k}'_\parallel} &= \int_{\mathbb{R}} \int_{\mathbb{R}} dx \, dx' \, \psi_{j,a}^{(s)}(x) \, U_K^{\mathbf{k}_\parallel \mathbf{k}'_\parallel}(x,x') \, \psi_{j,0}^{(t)}(x') \\ &= \frac{4\pi}{V_{SC}} \, 2^{-j} \sum_{q_1}{}' \frac{e^{i2^{-j} a q_1}}{q_1^2 + |\mathbf{k}_\parallel - \mathbf{k}'_\parallel|^2} \, \hat{\psi}^{(s)}(2^{-j}q_1)^* \, \hat{\psi}^{(t)}(2^{-j}q_1). \end{aligned} \tag{84}$$

In the following we assume $|\mathbf{k}_\parallel - \mathbf{k}'_\parallel| > 0$, otherwise we would just recover the effective Coulomb potential (78). Due to the absence of an infrared divergence in this case, we can perform the continuum limit for the effective exchange kernel (83)

$$U_K^{\mathbf{k}_\parallel \mathbf{k}'_\parallel}(x,x') = \frac{2\pi}{A_{SC}} \frac{e^{-|\mathbf{k}_\parallel - \mathbf{k}'_\parallel| \, |x-x'|}}{|\mathbf{k}_\parallel - \mathbf{k}'_\parallel|}, \tag{85}$$

which has allready been stated in Bardeen's early paper [5]. It can be seen from Fig. 4 a) that pure scaling function integrals are very good approximated by the continuum Eq. (85) over the whole range of momenta $|\mathbf{k}_\parallel - \mathbf{k}'_\parallel|$. Close to the diagonal, the intermediate exchange integrals involving wavelets behave rather similar to the Coulomb case, as it is shown in Fig. 4 b). Obviously this is due to the fact that, up to a constant term, both effective potentials have in leading order the same asymptotic behaviour close to the diagonal. This leading order term $\sim |x-x'|$ determines the regularity of the effective potentials on the diagonal and thereby the magnitude of the wavelet integrals. At larger distances from the diagonal, an exponential decay can be observed depending on the total parallel momentum $|\mathbf{k}_\parallel - \mathbf{k}'_\parallel|$.

Intermediate Coulomb and exchange integrals for jellium slabs can be directly computed using Eqs. (79) and (84). The reciprocal lattice sums converge fast depending on the decay properties of the Fourier transform of scaling function and wavelet. For more general cases, discussed in Section 3, the computation of intermediate integrals is much more involved and leads to additional approximation errors. We just want

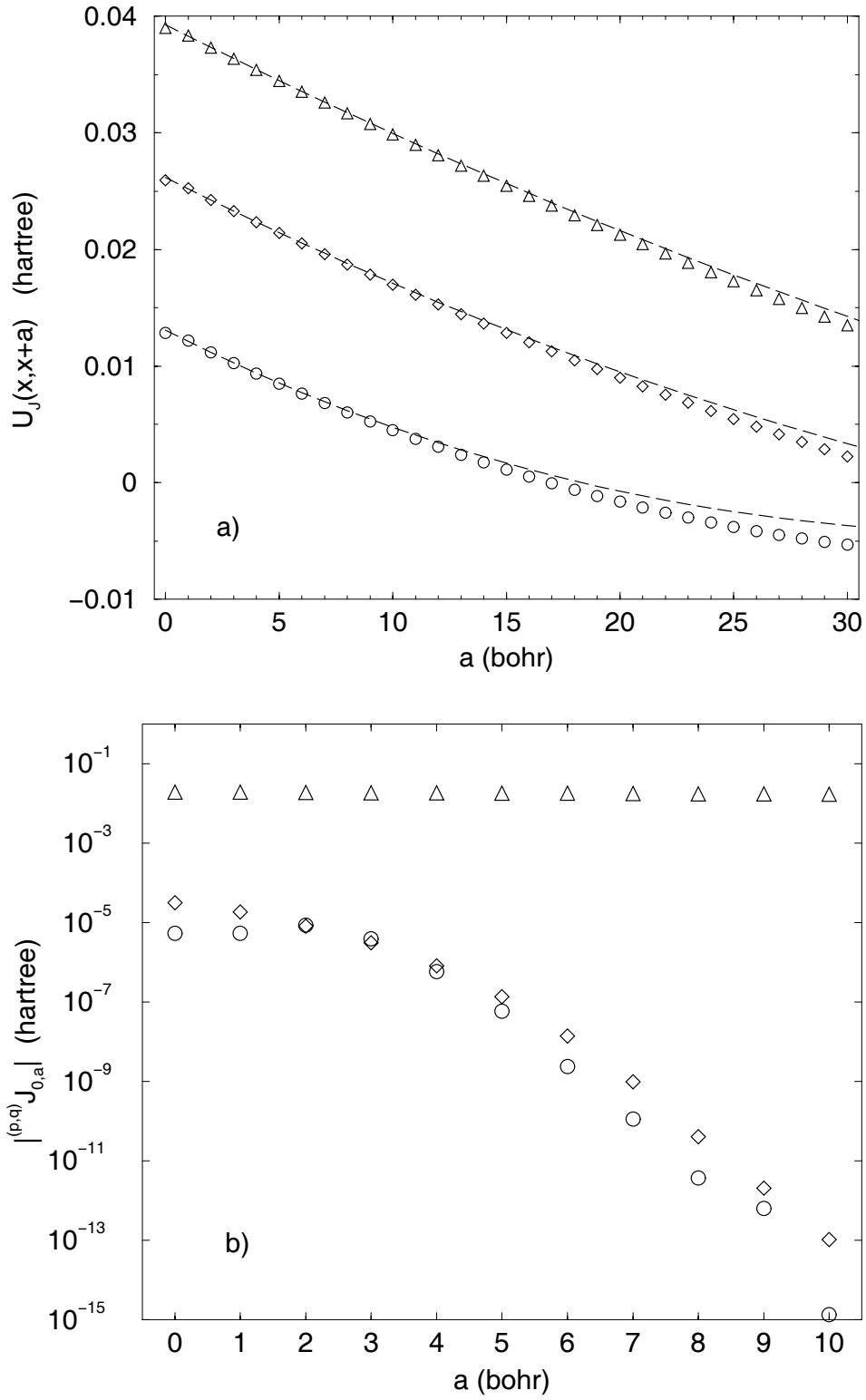

Figure 3: Intermediate Coulomb integrals for jellium slabs. a) Asymptotic effective potential $U_J(x, x+a)$ (dashed lines) and pure scaling function integrals ${}^{(0,0)}J_{0,a}$ for various size of the supercell ($D_2 = D_3 = 80$ bohr): ($\circ$) $D_1 = 80$ bohr, ($\diamond$) $D_1 = 160$ bohr, ($\triangle$) $D_1 = 240$ bohr. b) Different types of integrals: ($\triangle$) $|{}^{(0,0)}J_{0,a}|$ (pure scaling functions), ($\diamond$) $|{}^{(0,1)}J_{0,a}|$ (mixed scaling function and wavelet), ($\circ$) $|{}^{(1,1)}J_{0,a}|$ (pure wavelets) for a supercell of size $D_1 = 240$ bohr, $D_2 = D_3 = 80$ bohr. The integrals have been calculated for SDD6 wavelets and scaling functions.

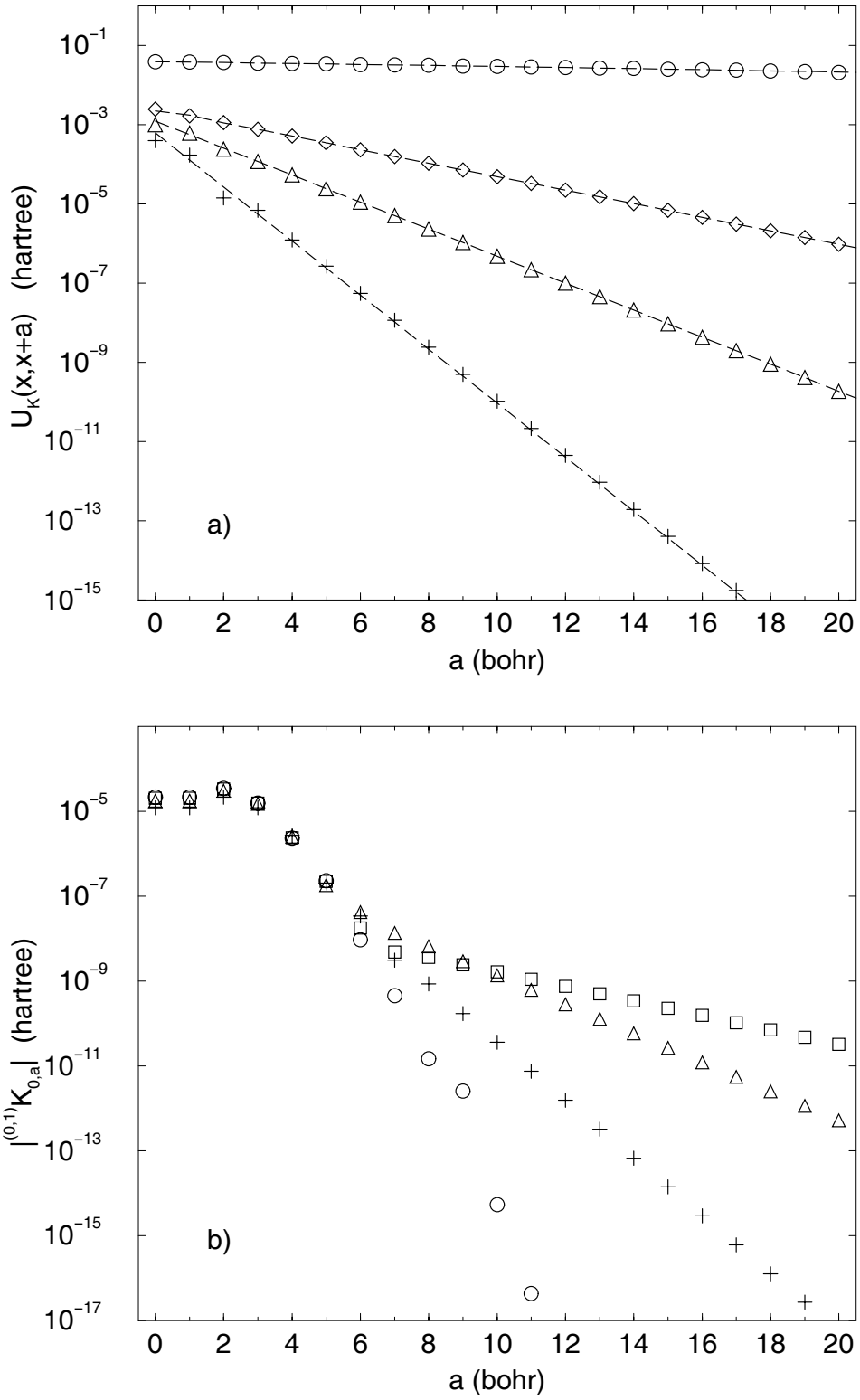

Figure 4: Intermediate exchange integrals for jellium slabs at different momenta $|\mathbf{k}_\parallel - \mathbf{k}'_\parallel|$: ($\circ$) 0 bohr^{-1}, ($\square$) 0.13 bohr^{-1}, ($\triangle$) 0.26 bohr^{-1}, ($+$) 0.52 bohr^{-1} (supercell size $D_1 = 240$ bohr, $D_2 = D_3 = 80$ bohr). a) Asymptotic effective potential $U_K^{\mathbf{k}_\parallel \mathbf{k}'_\parallel}(x, x+a)$ (dashed lines) and pure scaling function integrals ${}^{(0,0)}K_{0,a}^{\mathbf{k}_\parallel \mathbf{k}'_\parallel}$. b) Mixed scaling function and wavelet integrals $|{}^{(0,1)}K_{0,a}^{\mathbf{k}_\parallel \mathbf{k}'_\parallel}|$. The integrals have been calculated for SDD6 wavelets and scaling functions.

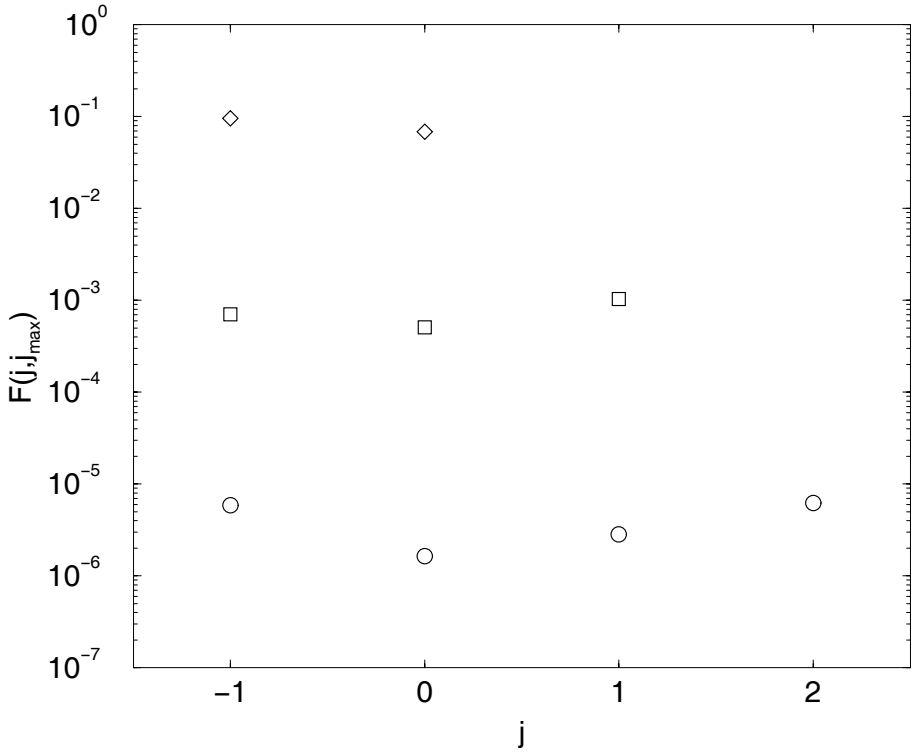

Figure 5: Approximation error for intermediate exchange integrals at different wavelet levels j. Relative errors in the Frobenius norm $F(j, j_{max})$ with $|\mathbf{k}_\parallel| \leq 3.7$ bohr^{-1} are shown for various values of the finest wavelet level j_{max}: ($\diamond$) 0, ($\square$) 1, ($\circ$) 2. The integrals have been calculated for SDD6 wavelets and scaling functions.

to draw attention on the wavelet products appearing in the expressions (48) and (49) for these integrals. It should be emphasized however, that all approximation errors can be controlled in a systematic way, in order to achieve certain absolute or relative accuracies. The jellium model provides an independent test for the numerical accuracy of the general algorithm. Contributions from fine wavelet levels are truncated in Eq. (56) at a level j_{max}. This constitutes the essential approximation error in our scheme, which is based on the nonstandard evaluation of integrals. We have considered relative errors of intermediate exchange integrals (49) at different wavelet levels j in the Frobenius norm

$$F(j, j_{max})^2 := \frac{\sum_{\mathbf{k}_\parallel, \mathbf{k}'_\parallel} \sum_{s,t} \sum_a \left| {}^{(s,t)}K_{j,a}^{\mathbf{k}_\parallel \mathbf{k}'_\parallel}(j_{max}) - {}^{(s,t)}K_{j,a}^{\mathbf{k}_\parallel \mathbf{k}'_\parallel}(\infty) \right|^2}{\sum_{\mathbf{k}_\parallel, \mathbf{k}'_\parallel} \sum_{s,t} \sum_a \left| {}^{(s,t)}K_{j,a}^{\mathbf{k}_\parallel \mathbf{k}'_\parallel}(\infty) \right|^2}, \tag{86}$$

where the argument j_{max} denotes the finest wavelet level in Eq. (56) and ∞ indicates the use of Eq. (84). Convergence of the relative Frobenius error with respect to j_{max} is very fast and almost independent of j, as can be seen from Fig. 5. Typically, the errors are reduced by two orders of magnitude by incorporating the next finer wavelet level in Eq. (56).

6.1 Numerical studies for a homogeneous electron gas

In order to study the numerical accuracy of our method, we considered the homogeneous electron gas, which corresponds to the limiting case of a jellium slab filling up the whole supercell. Beside HF energies at various electron densities, we have also considered Frobenius errors for the exchange part of the Fock matrix. Due to the definition of the Ewald potential, the Coulomb part (46) of the Fock matrix vanishes for

Table 1: Hartree-Fock energies per electron (hartree) of a homogeneous electron gas at various densities and supercell size. The relative Frobenius errors (F) of the exchange part of the Fock matrix have been calculated according to Eq. (86). SDD6 wavelets and scaling functions have been used for these calculations.

r_s	N_e	D^a	j^b	${j_{max}}^c$	E_{HF}	${E_{\text{exact}}}^d$	ΔE	$F(j, j_{max})$
0.5	114	4	1	2	1.57884880	1.57884476	4.0×10^{-6}	3.6×10^{-5}
1	114	8	0	1	0.25373817	0.25373662	1.6×10^{-6}	3.6×10^{-5}
2	114	16	-1	0	-0.00705256	-0.00705313	5.7×10^{-7}	3.6×10^{-5}
4	114	32	-2	-1	-0.03700668	-0.03700693	2.5×10^{-7}	3.6×10^{-5}

[a] Length of the supercell (bohr).
[b] Finest level of the wavelet expansion.
[c] Finest wavelet level in Eq. (56).
[d] Exact HF energy.

a homogeneous electron gas. The remaining exchange matrix elements (47) can be directly obtained by first integrating out the parallel directions, analogously to the case of intermediate integrals (84). Integration in the perpendicular direction yields a one dimensional reciprocal lattice sum, which converges reasonably fast to be summed up numerically. A straightforward calculation, using the effective kernel (83), yields the following expression for exchange matrix elements in a supercell wavelet basis

$$\begin{aligned} {}^{(s,t)}K_{ja,lb}^{\kappa_1,\mathbf{k}_\parallel} &= \frac{1}{L_{SC}} \sum_{\mathbf{k}'} \int_{L_{SC}} \int_{L_{SC}} dx\, dx'\, \mathcal{R}\psi_{j,a}^{(s)\kappa_1}(x)^*\, e^{ik_1' x}\, U_K^{\mathbf{k}_\parallel \mathbf{k}'_\parallel}(x,x')\, e^{-ik_1' x'}\, \mathcal{R}\psi_{l,b}^{(t)\kappa_1}(x') \qquad (87) \\ &= \frac{1}{L_{SC}} \sum_{\mathbf{k}'} \int_{\mathbb{R}} \int_{\mathbb{R}} dx\, dx'\, \psi_{j,a}^{(s)\kappa_1}(x)^*\, e^{ik_1' x}\, U_K^{\mathbf{k}_\parallel \mathbf{k}'_\parallel}(x,x')\, e^{-ik_1' x'}\, \psi_{l,b}^{(t)\kappa_1}(x') \\ &= \mathcal{N}_{j,l} \sum_{\mathbf{k}'} {\sum_{q_1}}' \delta_{q_1|_j,\kappa_1}\, \delta_{q_1|_l,\kappa_1} \frac{e^{i(2^{-j}a - 2^{-l}b)q_1}}{|q_1 - k_1'|^2 + |\mathbf{k}_\parallel - \mathbf{k}'_\parallel|^2}\, \hat{\psi}^{(s)}(2^{-j}q_1)^* \hat{\psi}^{(t)}(2^{-l}q_1), \end{aligned}$$

where the constant

$$\mathcal{N}_{j,l} = \frac{4\pi}{V_{SC}}\, 2^{-\max\{j+u_1,0\}/2}\, 2^{-\max\{l+u_1,0\}/2} \qquad (88)$$

depends on the wavelet levels j, l. In Fig. 6 we have plotted exchange matrix elements (87) versus the distance of the wavelet centers $2^{-j}|a-b|$. After an initial exponential decay, these matrix elements approach almost constant values. This is due to the fact that the reduced one-particle density matrix for a homogeneous electron gas has an oscillatory behaviour and decays only algebraically with respect to the inter-electron distance. At sufficiently large distances, the Coulomb singularity does not contribute to the integral (87) any more. Therefore, it is the oscillatory behaviour of the density matrix which determines the magnitude of exchange matrix elements at large distances [19]. Nevertheless, the absolute magnitudes of these matrix elements are rather small and decay very fast with respect to the wavelet level j, as can be seen from Fig. 6.

We have calculated relative errors for the exchange matrix (47) in the Frobenius norm (86) together with HF energies per electron at electron densities $r_s = 0.5, 1, 2,$ and 4 for supercells containing 114 electrons. It can be seen from Table 1 that we obtain relative errors of $\approx 10^{-5}$ for the exchange matrix by choosing a wavelet discretization comparable to the mean radius per electron r_s. This corresponds to absolute errors of $\approx 10^{-6}$ hartree for the energy per electron. The test calculations for a homogeneous electron gas demonstrate the computational feasibility of our approach.

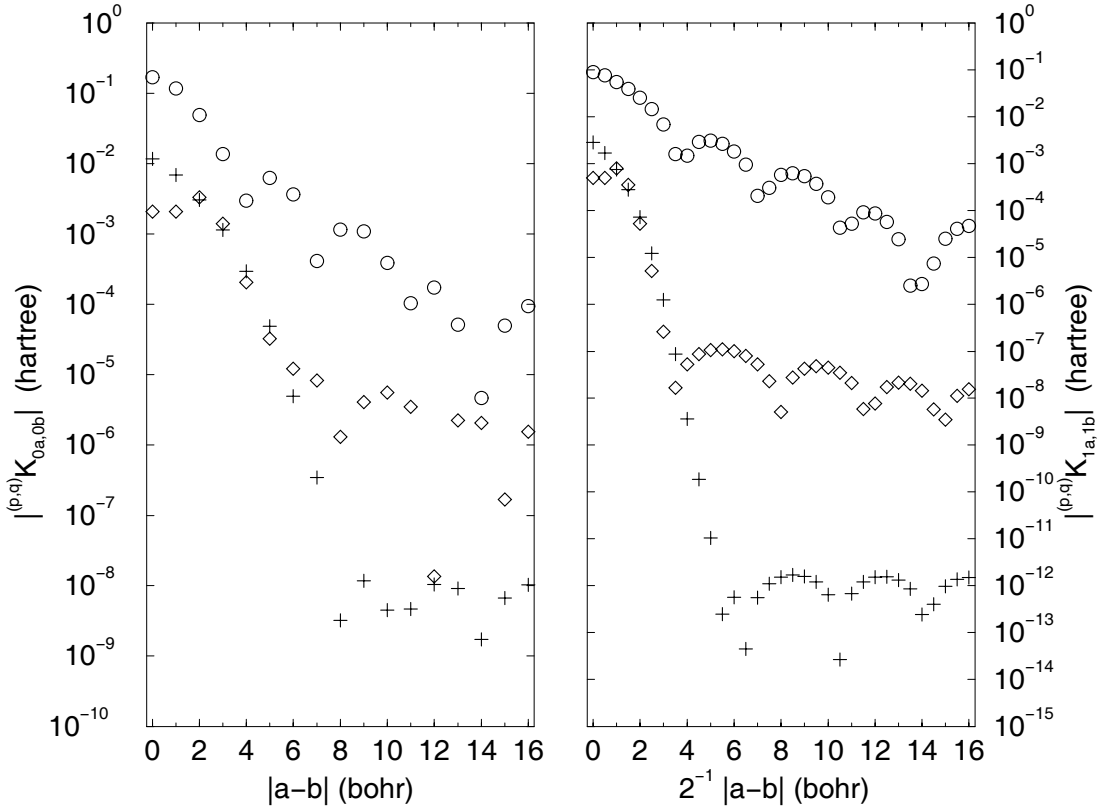

Figure 6: Exchange matrix elements ($|k_{\|}| = 0$ bohr^{-1}) for a homogeneous electron gas (87) with Fermi momentum $k_F = 2$ bohr^{-1}. Different types of matrix elements are plotted versus the distance of the wavelet centers $2^{-j}|a-b|$: ($\circ$) $|^{(0,0)}K^{0,\mathbf{0}}_{ja,jb}|$ (pure scaling functions), ($\diamond$) $|^{(0,1)}K^{0,\mathbf{0}}_{ja,jb}|$ (mixed scaling function and wavelet), ($+$) $|^{(1,1)}K^{0,\mathbf{0}}_{ja,jb}|$ (pure wavelets). Left and right parts of the figure correspond to levels $j = 0$ and $j = 1$, respectively. A supercell ($D_1 = D_2 = D_3 = 32$ bohr) which consists of a single unit cell has been chosen. Matrix elements have been calculated for SDD6 wavelets and scaling functions.

7 Conclusions

Many interesting developments in modern physics and chemistry originate from the peculiar properties of quasi two-dimensional systems. Due to their strongly anisotropic behaviour in one direction, these systems present a great challenge to numerical simulations. The inherent two-scale character of the problem suggests an application of recently developed numerical techniques in multiresolution analysis. We have studied a multiresolution HF approach to quasi two-dimensional systems based on wavelets and low rank tensor product expansions. The method has been tailored for systems where the coupling between the anisotropic and isotropic directions is rather weak. This is definitely the case for jellium slabs, which provide a guideline for such kind of systems. Thin jellium slabs and related systems, like excitons in quantum wells, are often considered as purely two-dimensional systems. For certain applications this is not really appropriate from a physical point of view. Nevertheless, we can use these results as a guiding principle for the construction of a tensor product basis. This is similar to the highly successful linear combination of atomic orbitals approach in molecular physics. We further follow along this line for the construction of the Fock matrix, which comprises the most expensive part of a HF calculation. The physical insight concerning the homogeneous directions of the system has been expressed in terms of intermediate exchange and Coulomb integrals. These integrals do not change during the self-consistent solution of the HF equation. As a consequence, we can essentially restrict the necessary update of the Fock matrix, during each iteration, to the anisotropic part of the orbitals. The intermediate integrals have

sparse representations in a wavelet basis, which enable an efficient computation of the Fock matrix.

Although, the present work is in particular limited to the HF approach, it also has some consequences for post HF methods. Accurate HF wavefunctions usually serve as a starting point for many-particle methods, where correlated wavefunctions are expressed through correlation operators acting on a Slater determinant. Furthermore, we want to emphasize that our numerical techniques, originally developed for the exchange part of the Fock operator, provide a foundation for the evaluation of more general integrals, required by many-particle methods, as it has been discussed in Ref. [19]. Another possible application of HF wavefunctions are QMC calculations, where Slater determinants form a part of the trial wavefunction. This seems to be especially promising with respect to the high demands on the numerical accuracy of trial wavefunctions in QMC calculations for strongly anisotropic systems.

8 Acknowledgments

The authors gratefully acknowledge Dr. T. Koprucki (Berlin) and Prof. H. Stoll (Stuttgart) for useful discussions. This work was supported by the Deutsche Forschungsgemeinschaft (SPP 1095).

Appendices

A Basic notions of multiresolution analysis

The purpose of this appendix is to provide some basic definitions and properties of wavelets in order to make the paper fairly self-contained. We give a brief discussion of multiresolution analysis in one dimension and provide some basic notions for the multi-dimensional case. For further details the reader is referred e.g. to Refs. [10, 11, 22, 38], which present excellent introductions into the subject. Multiresolution analysis leads to a decomposition of the Hilbert space $L^2(\mathbb{R})$ into an infinite sequence of ascending subspaces $\cdots \subset V_{j-1} \subset V_j \subset V_{j+1} \subset \cdots$, where the index j runs over all integers. The union of these subspaces $\bigcup_j V_j$ is dense in $L^2(\mathbb{R})$. On each subspace V_j, the mother scaling function $\varphi(x)$ provides a basis

$$\varphi_{j,a}(x) := 2^{j/2}\varphi(2^j x - a) \tag{89}$$

via the operations of dilation and translation. The dilation factor 2^j scales the size of the basis functions, which means that with increasing j, the $\varphi_{j,a}$ provide a finer resolution in L^2. An explicit embedding of V_j into the larger space V_{j+1} is given by the refinement relation

$$\varphi_{j,a}(x) = 2^{1/2} \sum_b h_{b-2a}\, \varphi_{j+1,b}(x), \tag{90}$$

where the number of filter coefficients h_a is finite for the scaling functions used in our applications. Wavelet spaces W_j are defined as complements of V_j in V_{j+1}, where the corresponding wavelet basis is generated from a mother wavelet $\psi(x)$ analogously to Eq. (89)

$$\psi_{j,a}(x) := 2^{j/2}\psi(2^j x - a). \tag{91}$$

A refinement relation similar to Eq. (90)

$$\psi_{j,a}(x) = 2^{1/2} \sum_b g_{b-2a}\, \varphi_{j+1,b}(x), \tag{92}$$

relates the mother wavelet to scaling functions on the next finer level. This construction leads to a hierarchical decomposition of $L^2 = \bigoplus_{l\in\mathbb{Z}} W_l$ into wavelet subspaces W_l [11]. Sometimes it is convenient to use common symbols for scaling functions and wavelets

$$\psi^{(0)}_{j,a}(x) := \varphi_{j,a}(x), \qquad \psi^{(1)}_{j,a}(x) := \psi_{j,a}(x). \tag{93}$$

We freely adopt to this notation whenever it seems to be beneficial. In a biorthogonal wavelet basis there exists a sequence of dual spaces $\tilde{V}_j$, $\tilde{W}_j$, which satisfy the orthogonality relations $\tilde{W}_j \perp V_j$ and $\tilde{V}_j \perp W_j$. The corresponding dual wavelets $\tilde{\psi}_{j,a} := 2^{j/2}\tilde{\psi}(2^j x - a)$ and scaling functions $\tilde{\varphi}_{j,a} := 2^{j/2}\tilde{\varphi}(2^j x - a)$ provide a biorthogonal basis in L^2

$$\langle \varphi_{j,a} | \tilde{\varphi}_{j,b} \rangle = \delta_{a,b}, \qquad \langle \psi_{j,a} | \tilde{\psi}_{l,b} \rangle = \delta_{j,l}\, \delta_{a,b}. \tag{94}$$

The sparsity of wavelet approximations is due to the vanishing moment property

$$\int dx\, x^k\, \psi(x) = 0, \text{ for } \; k = 0, \ldots, n-1. \tag{95}$$

This property leads to a vast decay of wavelet coefficients for smooth functions with respect to the level of refinement. Furthermore, it enables sparse representations of singular kernel functions, like Coulomb potentials, that satisfy the asymptotic smoothness condition [7, 8]. For our numerical studies, we have used the univariate biorthogonal wavelets with six vanishing moments of Sweldens [59], based on the interpolating scaling function of Deslauriers and Dubuc [12]. In the text, we refer to this basis as the SDD6 wavelet basis.

Isotropic 2d- and 3d-wavelets have been used for the construction of basis functions in the parallel directions and for the wavelet representation of Ewald potentials, respectively. These wavelets are obtained by taking mixed tensor products of univariate wavelets $\psi_{j,a}$ and scaling functions $\varphi_{j,a}$ on the same level j. In the 2d case, beside scaling functions

$$\gamma^{(0)}_{j,\mathbf{a}_\parallel}(\mathbf{r}_\parallel) = \varphi_{j,a_2}(y)\, \varphi_{j,a_3}(z), \tag{96}$$

there are three different types of isotropic wavelets

$$\begin{aligned} \gamma^{(1)}_{j,\mathbf{a}_\parallel}(\mathbf{r}_\parallel) &= \psi_{j,a_2}(y)\, \varphi_{j,a_3}(z), \\ \gamma^{(2)}_{j,\mathbf{a}_\parallel}(\mathbf{r}_\parallel) &= \varphi_{j,a_2}(y)\, \psi_{j,a_3}(z), \\ \gamma^{(3)}_{j,\mathbf{a}_\parallel}(\mathbf{r}_\parallel) &= \psi_{j,a_2}(y)\, \psi_{j,a_3}(z). \end{aligned} \tag{97}$$

Correspondingly in the 3d case, isotropic scaling functions and wavelets are given by

$$\begin{aligned} \gamma^{(0)}_{j,\mathbf{a}}(\mathbf{r}) &= \varphi_{j,a_1}(x)\, \varphi_{j,a_2}(y)\, \varphi_{j,a_3}(z), \\ \gamma^{(1)}_{j,\mathbf{a}}(\mathbf{r}) &= \psi_{j,a_1}(x)\, \varphi_{j,a_2}(y)\, \varphi_{j,a_3}(z), \\ &\vdots \\ \gamma^{(4)}_{j,\mathbf{a}}(\mathbf{r}) &= \psi_{j,a_1}(x)\, \psi_{j,a_2}(y)\, \varphi_{j,a_3}(z), \\ &\vdots \\ \gamma^{(7)}_{j,\mathbf{a}}(\mathbf{r}) &= \psi_{j,a_1}(x)\, \psi_{j,a_2}(y)\, \psi_{j,a_3}(z). \end{aligned} \tag{98}$$

According to this scheme, the scaling functions $\gamma^{(0)}_{j,\mathbf{a}}$ and wavelets $\gamma^{(1)}_{j,\mathbf{a}}$, $\gamma^{(2)}_{j,\mathbf{a}} \ldots$ belong to well defined levels j. However, the various types of isotropic wavelets might have otherwise different properties. Sometimes it becomes necessary to specify for an isotropic wavelet $\gamma^{(p)}_{j,\mathbf{a}}$, the type of function $\psi^{(p_i)}_{j,a_i}$ in a specific direction. According to our notation (93), $p_i = 0, 1$, depending whether there is a scaling function or a wavelet.

Filter coefficients for multiscale relations of bilinear forms are required in Eq. (56). These coefficients can be obtained from the two-scale relations

$$\int dx_1 dx_2\, \psi^{(p)}_{j,a}(x_1)\, f(|x_1 - x_2|)\, \psi^{(q)}_{j,0}(x_2) = \sum_b {}^{(p,q)}H_{b-2a} \int dx_1 dx_2\, \psi^{(0)}_{j+1,b}(x_1)\, f(|x_1 - x_2|)\, \psi^{(0)}_{j+1,0}(x_2), \tag{99}$$

with

$$ {}^{(0,0)}H_b := 2\sum_c h_{b+c}h_c, \quad {}^{(1,0)}H_b := 2\sum_c g_{b+c}h_c, \quad \text{etc.} \tag{100} $$

Recursive application of the two-scale relations

$$ {}^{(p,q)}H_b^2 = \sum_c {}^{(p,q)}H_c \, {}^{(0,0)}H_{b-2c}, \tag{101} $$

$$ {}^{(p,q)}H_b^3 = \sum_c {}^{(p,q)}H_c^2 \, {}^{(0,0)}H_{b-2c}, \tag{102} $$

$$ \vdots \tag{103} $$

provides multiscale filter coefficients to arbitrary fine levels.

B Refinement relations for periodic wavelets and scaling functions

In order to complete our discussion of supercell wavelets in Section 2.1, we provide here refinement relations for periodically extended supercell wavelets and scaling functions. Since from a formal point of view, the refinement relations for wavelets and scaling functions are completely equivalent, we restrict ourselves to scaling functions. The ordinary two-scale refinement relation for scaling functions (90) extends to the periodic setting for the cases $j + u_i \geq 0$ and $j + u_i < 0$, differently. Here u_i relates to the unit cell lattice vectors (7). To simplify our notation, we drop the directional index i in the following. In the case $j + u \geq 0$, straightforward application of Eq. (90), together with $t_{j,n} = t_{j+1,n}$, $M_j = M_{j+1}$ and $\Omega_j = \Omega_{j+1}$, cf. Eqs. (14), (15) and (16), yields the refinement relation for periodically extended supercell scaling functions

$$ \begin{aligned} \mathcal{R}\varphi^{\kappa}_{j,a}(x) &= 2^{1/2}\sum_{b\in\mathbb{Z}} h_{b-2a}\,\mathcal{R}\varphi^{\kappa}_{j+1,b}(x) \\ &= 2^{1/2}\sum_{c\in\Lambda_{j+1}} \left(\sum_{m\in\mathbb{Z}} h_{2^{j+1}t_{j+1,m}+c-2a}\, e^{-i\kappa t_{j+1,m}}\right) \mathcal{R}\varphi^{\kappa}_{j+1,c}(x) \\ &= 2^{1/2}\sum_{c\in\Lambda_{j+1}} h^{\kappa}_{j+1,c-2a}\,\mathcal{R}\varphi^{\kappa}_{j+1,c}(x). \end{aligned} \tag{104} $$

Here we have introduced periodic filter coefficients

$$ h^{\kappa}_{j,a} = \sum_{m\in\mathbb{Z}} h_{2^j t_{j,m}+a}\, e^{-i\kappa t_{j,m}}, \tag{105} $$

in order to obtain a compact notation. The corresponding relation in the case $j + u < 0$ is of the form

$$ \mathcal{R}\varphi^{\kappa}_{j,0}(x) = h^{\kappa'}_{j+1,0}\,\mathcal{R}\varphi^{\kappa'}_{j+1,0}(x) + h^{\kappa}_{j+1,0}\,\mathcal{R}\varphi^{\kappa}_{j+1,0}(x), \tag{106} $$

where a linear combination of two supercell scaling functions appears, which belong to two different wave vectors

$$ \kappa' = \frac{2\pi}{2^u N}\left(n + \frac{M_{j+1}}{2}\right) \text{ and } \kappa = \frac{2\pi}{2^u N}\, n. \tag{107} $$

This is due to the fact that the first wave vector coincides with the second after reduction to the first BZ on level j, i.e. $\kappa'|_j = \kappa$. Furthermore we have used $t_{j,n} = 2t_{j+1,n}$ and $M_{j+1} = 2M_j$ for the derivation of the refinement relation (106), cf. Eqs. (14), (15) and (16).

C Symmetry relations for symmetric biorthogonal wavelet bases

The usage of symmetric biorthogonal wavelet bases for the representation of translational invariant kernel functions, like interaction potentials, allows for some additional savings with respect to storage requirements. In order to employ symmetry, we have to bear in mind that seven different types of isotropic three-dimensional wavelets exist. Each type is centred on a regular lattice. These lattices, however, are shifted against one another. The consequences for the inversion symmetry of wavelet matrix elements of translational invariant kernel functions are most easily demonstrated for the Coulomb interaction. In the case of symmetric scaling functions and wavelets, the Coulomb matrix elements

$$\langle \gamma^{(p)}_{j,\mathbf{a}} | \frac{1}{r_{12}} | \gamma^{(q)}_{j,\mathbf{0}} \rangle := \int_{\mathbb{R}^3} \int_{\mathbb{R}^3} d^3r_1 d^3r_2 \, \gamma^{(p)}_{j,\mathbf{a}}(\mathbf{r}_1) \, \frac{1}{|\mathbf{r}_1 - \mathbf{r}_2|} \, \gamma^{(q)}_{j,\mathbf{0}}(\mathbf{r}_2), \tag{108}$$

satisfy inversion relations

$$\langle \gamma^{(p)}_{j,-\mathbf{a}} | \frac{1}{r_{12}} | \gamma^{(q)}_{j,\mathbf{0}} \rangle = \langle \gamma^{(p)}_{j,\mathbf{a}+\mathbf{s}_{(p,q)}} | \frac{1}{r_{12}} | \gamma^{(q)}_{j,\mathbf{0}} \rangle, \tag{109}$$

with shift vectors

$$s_{(p,q)_i} := \begin{cases} 0 & \text{if } (p_i, q_i) = (0,0) \\ 1 & \text{if } (p_i, q_i) = (0,1) \\ -1 & \text{if } (p_i, q_i) = (1,0) \\ 0 & \text{if } (p_i, q_i) = (1,1) \end{cases}, \tag{110}$$

depending on the specific combinations of wavelets and scaling functions in each direction. The inversion relations hold for each component of the vector $\mathbf{a}$ separately. Therefore, the storage requirement for Coulomb matrix elements are reduced by a factor of eight.

In order to make use of symmetry for the Ewald potential, we have to consider a combination of translation and inversion symmetry. The translational symmetry of the Ewald potential manifests itself in the relation

$$U_{\text{Ewald}}(\mathbf{r}_1, \mathbf{r}_2) = U_{\text{Ewald}}(\mathbf{r}_1 + \mathbf{R}_n, \mathbf{r}_2) = U_{\text{Ewald}}(\mathbf{r}_1, \mathbf{r}_2 + \mathbf{R}_n), \tag{111}$$

which immediately yields the corresponding relation for the wavelet matrix elements

$$\langle \gamma^{(p)}_{j,\mathbf{a}+2^j\mathbf{R}_n} | U_{\text{Ewald}} | \gamma^{(q)}_{j,\mathbf{0}} \rangle = \langle \gamma^{(p)}_{j,\mathbf{a}} | U_{\text{Ewald}} | \gamma^{(q)}_{j,\mathbf{0}} \rangle. \tag{112}$$

According to Eq. (112), we can substitute $-\tilde{a}_i \to a_i$ with $\tilde{a}_i = 2^{j+u_i} N_i - a_i$ in the Ewald matrix elements and use Eq. (109) to obtain the symmetry relation

$$\langle \gamma^{(p)}_{j,\mathbf{a}} | U_{\text{Ewald}} | \gamma^{(q)}_{j,\mathbf{0}} \rangle = \langle \gamma^{(p)}_{j,-\tilde{\mathbf{a}}} | U_{\text{Ewald}} | \gamma^{(q)}_{j,\mathbf{0}} \rangle = \langle \gamma^{(p)}_{j,\tilde{\mathbf{a}}+\mathbf{s}_{(p,q)}} | U_{\text{Ewald}} | \gamma^{(q)}_{j,\mathbf{0}} \rangle. \tag{113}$$

Therefore, Ewald matrix elements are invariant with respect to the substitution

$$\tilde{\mathbf{a}} + \mathbf{s}_{(p,q)} \to \mathbf{a}. \tag{114}$$

Let us assume that

$$2^{j+u_i-1} N_i + s_{(p,q)_i}/2 < a_i < 2^{j+u_i} N_i. \tag{115}$$

From the definition of $\tilde{a}_i$ and inequality (115), we obtain

$$s_{(p,q)_i} < \tilde{a}_i + s_{(p,q)_i} < 2^{j+u_i-1} N_i + s_{(p,q)_i}/2. \tag{116}$$

As a consequence of this inequality only Ewald matrix elements with

$$\max(s_{(p,q)_i}, 0) \le a_i \le 2^{j+u_i-1} N_i + s_{(p,q)_i}/2 \tag{117}$$

have to be calculated and stored. Due to translation-inversion symmetry, the storage requirements for Ewald potentials reduce by a factor of eight.

References

[1] P.H. Acioli and D.M. Ceperley, Diffusion Monte Carlo study of jellium surfaces: Electronic densities and pair correlation functions, Phys. Rev. B **54**, No. 23, 17199 (1996).

[2] L.M. Almeida, J.P. Perdew and C. Fiolhais, Surface and curvature energies from jellium spheres: Density functional hierarchy and quantum Monte Carlo, Phys. Rev. B **66**, No. 7, 075115 (2002).

[3] T.A. Arias, *Multiresolution analysis of electronic structure: Semicardinal and wavelet bases*, Rev. Mod. Phys. **71** No. 1, 267 (1999).

[4] P.Y. Ayala, K.N. Kudin and G.E. Scuseria, Atomic orbital Laplace-transformed second-order Møller-Plesset theory for periodic systems, J. Chem. Phys. **115**, No. 21, 9698 (2001).

[5] J. Bardeen, Theory of the work function II. The surface double layer, Phys. Rev. **49**, No. 9, 653 (1936).

[6] G. Bastard, E.E. Mendez, L.L. Chang and L. Esaki, Variational calculations on a quantum well in an electric field, Phys. Rev. B **28**, No. 6, 3241 (1983).

[7] G. Beylkin, On the representation of operators in bases of compactly supported wavelets, SIAM J. Numer. Anal. **6**, No. 6, 1716 (1992).

[8] G. Beylkin, R.R. Coifman and V. Rokhlin, Fast wavelet transforms and numerical algorithms I, Commun. Pure Appl. Math. **44**, No. 2, 141 (1991).

[9] S.L. Chuang, *Physics of Optoelectronic Devices*, (Wiley, New York, 1995).

[10] W. Dahmen, Wavelet and multiscale methods for operator equations, Acta Numerica **6**, 55 (1997).

[11] I. Daubechies, *Ten Lectures on Wavelets*, CBMS-NSF Regional Conference Series in Applied Mathematics **61** (SIAM, Philadelphia, 1992)

[12] G. Deslauriers and S. Dubuc, Symmetric iterative interpolation processes, Constr. Approx. **5**, No. 1, 49 (1989).

[13] J.F. Dobson, J. Wang and T. Gould, Correlation energies of inhomogeneous many-electron systems, Phys. Rev. B **66**, No. 8, 081108 (2002).

[14] T.D. Engeness and T.A. Arias, Multiresolution analysis for efficient, high precision all-electron density-functional calculations, Phys. Rev. B **65**, No. 16, 165106 (2002).

[15] R.A. Evarestov, S. Piskunov, E.A. Kotomin and G. Borstel, Single impurities in insulators: *Ab initio* study of Fe-doped $SrTiO_3$, Phys. Rev. B **67**, No. 6, 064101 (2003).

[16] R.A. Evarestov and V.P. Smirnov, Special points of the Brillouin zone and their use in the solid state theory, Phys. Status Solidi b **119**, No. 1, 9 (1983).

[17] R.A. Evarestov and V.P. Smirnov, Symmetrical transformation of basic translation vectors in the supercell model of imperfect crystals and in the theory of special points of the Brillouin zone, J. Phys.: Condens. Matter **9**, No. 14, 3023 (1997).

[18] H.-J. Flad, W. Hackbusch, D. Kolb and R. Schneider, Wavelet approximation of correlated wavefunctions. I. Basics, J. Chem. Phys. **116**, No. 22, 9641 (2002).

[19] H.-J. Flad, W. Hackbusch, H. Luo and D. Kolb, Toward diagrammatic multiresolution analysis for electron correlations, MPI-PKS preprint (2004).

[20] W.M.C. Foulkes, L. Mitas, R.J. Needs, G. Rajagopal, Quantum Monte Carlo simulations of solids, Rev. Mod. Phys. **73**, No. 1, 33 (2001).

[21] C. Freyria-Fava, R. Dovesi, V.R. Saunders, M. Leslie and C. Roetti, Ca and Be substitution in bulk MgO: *ab initio* Hartree-Fock and ionic model supercell calculations, J. Phys.: Condens. Matter **5**, No. 27, 4793 (1993).

[22] S. Goedecker, *Wavelets and their Application for the Solution of Differential Equations*, (Presses Polytechniques Universitaires et Romandes, Lausanne, 1998).

[23] M.K. Harbola and V. Sahni, Structure of the Fermi hole at surfaces, Phys. Rev. B **37**, No. 2, 745 (1988).

[24] J. Harris and R.O. Jones, The surface energy of a bounded electron gas, J. Phys. F: Metal Phys. **4**, 1170 (1974).

[25] R.J. Harrison, G.I. Fann, T. Yanai and G. Beylkin, Multiresolution quantum chemistry in multiwavelet bases, in *Computational Science - ICCS 2003*, LNCS **2660**, Eds. P.M.A. Sloot et al. (Springer, Berlin, 2003) p. 103.

[26] T. Helgaker, P. Jørgensen and J. Olsen, *Molecular Electronic-Structure Theory* (Wiley, New York, 1999).

[27] S. Hirata, R. Podeszwa, M. Tobita and R.J. Bartlett, Coupled-cluster singles and doubles for extended systems, J. Chem. Phys. **120**, No. 6, 2581 (2004).

[28] Y.Z. Hu, M. Lindberg and S.W. Koch, Theory of optically excited intrinsic semiconductor quantum dots, Phys. Rev. B **42**, No. 3, 1713 (1990).

[29] D.A. Kleinman, Binding energy of biexcitons and bound excitons in quantum wells, Phys. Rev. B **28**, No. 2, 871 (1983).

[30] E. Krotscheck and W. Kohn, Nonlocal screening in metal surfaces, Phys. Rev. Lett. **57**, No. 7, 862 (1986).

[31] E. Krotscheck, W. Kohn and G.-X. Qian, Theory of inhomogeneous quantum systems. IV. Variational calculations of metal surfaces, Phys. Rev. B **32**, No.9, 5693 (1985).

[32] N.D. Lang and W. Kohn, Theory of metal surfaces: Work functions, Phys. Rev. B **3**, No. 4, 1215 (1971).

[33] D.C. Langreth and J.P. Perdew, The exchange-correlation energy of a metallic surface, Solid State Commun. **17**, No. 11, 1425 (1975).

[34] X.-P. Li, R.J. Needs, R.M. Martin and D.M. Ceperley, Green's-function quantum Monte Carlo study of a jellium surface, Phys. Rev. B **45**, No. 11, 6124 (1992).

[35] A. Lichanot, Ph. Baranek, M. Mérawa, R. Orlando and R. Dovesi, V_{OH} and V_{OD} centers in alkaline-earth oxides: An *ab initio* supercell study, Phys. Rev. B **62**, No. 19, 12812 (2000).

[36] H. Luo, D. Kolb, H.-J. Flad, W. Hackbusch and T. Koprucki, Wavelet approximation of correlated wavefunctions. II. Hyperbolic wavelets and adaptive approximation schemes, J. Chem. Phys. **117**, No. 8, 3625 (2002).

[37] C.Q. Ma and V. Sahni, Study of the exchange energy of an inhomogeneous electron gas at a surface, Phys. Rev. B **20**, No. 6, 2291 (1979).

[38] S. Mallat, *A Wavelet Tour of Signal Processing* (Academic Press, San Diego, 1998).

[39] H.J. Monkhorst and J.D. Pack, Special points for Brillouin-zone integrations, Phys. Rev. B **13**, No. 12, 5188 (1976).

[40] J. Moreno and J.M. Soler, Optimal meshes for integrals in real- and reciprocal-space unit cells, Phys. Rev. B **45**, No. 24, 13891 (1992).

[41] M. Nekovee and J.M. Pitarke, Recent progress in the computational many-body theory of metal surfaces, Computer Phys. Comm. **137**, No. 1, 123 (2001).

[42] A.M.N. Niklasson, C.J. Tymczak and H. Röder, Multiresolution density-matrix approach to electronic structure calculations, Phys. Rev. B **66**, No. 15, 155120, (2002).

[43] R.S. Pfeiffer and H.B. Shore, Theory of donor-bound multiexciton complexes in germanium and silicon, Phys. Rev. B **25**, No. 6, 3897 (1982).

[44] C. Pisani, Ed., *Quantum-Mechanical Ab-initio Calculation of the Properties of Crystalline Materials*, Lecture Notes in Chemistry **67** (Springer, Berlin, 1996).

[45] J.M. Pitarke and A.G. Eguiluz, Jellium surface energy beyond the local-density approximation: Self-consistent-field calculations, Phys. Rev. B **63**, No. 4, 045116 (2001).

[46] J.M. Pitarke and J.P. Perdew, Metal surface energy: Persistent cancellation of short-range correlation effects beyond the random phase approximation, Phys. Rev. B **67**, No. 4, 045101 (2003).

[47] J. Puls, H.-J. Wünsche and F. Henneberger, Bi-excitons in wide-gap II-VI quantum wells. Localization by alloy disorder, Chem. Phys. **210**, Nos. 1-2, 235 (1996).

[48] G. Rajagopal, R.J. Needs, A. James, S.D. Kenny and W.M.C. Foulkes, Variational and diffusion quantum Monte Carlo calculations at nonzero wave vectors: Theory and application to diamond-structure germanium, Phys. Rev. B **51**, No. 16, 10591 (1995).

[49] G. Rajagopal, R.J. Needs, S. Kenny, W.M.C. Foulkes and A. James, Quantum Monte Carlo calculations for solids using special k-points methods, Phys. Rev. Lett. **73**, No. 14, 1959 (1994).

[50] A.A. Rogachev, Exciton molecules in multi-valley semiconductors, Prog. Quantum Electron. **25**, 141 (2001).

[51] V. Sahni and K.-P. Bohnen, Exchange charge density at metallic surfaces, Phys. Rev. B **29**, No. 2, 1045 (1984).

[52] V. Sahni and K.-P. Bohnen, Image charge at a metal surface, Phys. Rev. B **31**, No. 12, 7651 (1985).

[53] V. Sahni, J.B. Krieger and J. Gruenebaum, Metal surface properties in the linear potential approximation, Phys. Rev. B **15**, No. 4, 1941 (1977).

[54] V. Sahni and C.Q. Ma, Hartree-Fock theory of the inhomogeneous electron gas at a jellium metal surface: Rigorous upper bounds to the surface energy and accurate work functions, Phys. Rev. B **22**, No. 12, 5987 (1980).

[55] A. Shukla, M. Dolg, P. Fulde and H. Stoll, Obtaining Wannier functions of a crystalline insulator within a Hartree-Fock approach: Applications to LiF and LiCl, Phys. Rev. B **57**, No. 3, 1471 (1998).

[56] A. Shukla, M. Dolg, P. Fulde and H. Stoll, Wave-function-based correlated *ab initio* calculations on crystalline solids, Phys. Rev. B **60**, 5211 (1999).

[57] J.-Q. Sun and R.J. Bartlett, Second-order many-body perturbation-theory calculations in extended systems, J. Chem. Phys. **104**, No. 21, 8553 (1996).

[58] J.-Q. Sun and R.J. Bartlett, Convergence behavior of many-body perturbation theory with lattice summations in polymers, Phys. Rev. Lett. **80**, No. 2, 349 (1998).

[59] W. Sweldens, The lifting scheme: A custom-design construction of biorthogonal wavelets, Appl. Comput. Harmon. Anal. **3**, No. 2, 186 (1996).

[60] K.S. Thygesen, M.V. Bollinger and K.W. Jacobsen, Conductance calculations with a wavelet basis, Phys. Rev. B **67**, No. 11, 115404 (2003).

[61] A.I. Yakimov, N.P. Stepina, A.V. Dvurechenskii, A.I. Nikiforov and A.V. Nenashev, Many-particle effects in excitonic transitions in type-II Ge/Si quantom dots, Physica E **13**, Nos. 2-4, 1026 (2002).

[62] Z. Yan, J.P. Perdew, S. Kurth, C. Fiolhais and L. Almeida, Density functional versus wave-function methods: Toward a benchmark for the jellium surface energy, Phys. Rev. B **61**, No. 4, 2595 (2000); errata **64**, No. 4, 049904(E) (2001).

[63] Z.Y. Zhang, D.C. Langreth and J.P. Perdew, Planar-surface charge densities and energies beyond the local-density approximation, Phys. Rev. B **41**, No. 9, 5674 (1990).